Image processing based characterisation of coal cleat networks

J. Busse *[a], J.R. de Dreuzy [b], Sergio Galindo Torres [a], D. Bringemeier [a,c], A. Scheuermann [a]

*Corresponding author: j.busse@uq.edu.au, +61 40 1906 327

[a] Geotechnical Engineering Centre, School of Civil Engineering, University of Queensland, St. Lucia, QLD, Australia
[b] Geosciences Rennes, University Rennes 1, Rennes, Brittany, France
[c] Golder Associates Pty Ltd, Milton, QLD, Australia

Abstract

Characterisation of the cleat network serves as the basis for estimating the hydraulic and mechanical seam properties which in turn are fundamental for flow and geomechanical modelling in the context of underground coal mining. Cleat and cleat network geometry can be described as a function of frequency, aperture, size, orientation relative to in situ stresses, connectivity and porosity, with mineralised and un-mineralised cleats occurring. To describe these properties, CT-scans of core samples of a Bowen Basin coal in central Queensland, Australia, are analysed.

A unique image processing workflow method is introduced to extract the key statistical parameters of perpendicular butt and face cleats present in a two-dimensional image. As face and butt cleats have different characteristics, the presented method distinguishes face cleats and butt cleats by direction and present detailed data for both cleat types. The results comprise cleat length, apertures, sizes, intensities, densities, shape parameter, spacing, orientation and connectivity and are therefore more comprehensive than previous cleat descriptions. Three generally different cleat geometries are considered within this study, one sample shows perpendicular face and butt cleats, the second two sets of face cleats intersected by butt cleats and the third parallel face cleats only.

Keywords

cleat geometry, image processing, coal properties, CT scans

1. Introduction

1.1. *Coal cleat networks*

Coal is characterised by its unique microstructure of a low permeable porous matrix intersected by a network of face and butt cleats. Cleats are natural opening-mode fractures within coal beds. Together with fault related and mining induced large-scale fractures, these small scale cleats provide the principal source of permeability for groundwater and gas flow within the seam (Laubach et al., 1998). In contrast to the fractures, the smaller systematic cleats do not cut clastic facies adjacent to the coal layers (Dron 1925). Cleats are distinguished by their orientation into two types (Figure 1a). Face cleats are dominant and are directed perpendicular to the bedding plane. The fewer orthogonal butt cleats generally terminate when they encounter face cleats (Laubach et al., 1998). Butt cleats are thought to accommodate relaxation of the stress which originally formed the face cleats. This leads to perpendicularity between both cleat types (Golab et al. 2013). Most research has been done on this orthogonal cleat system. For example, Robertson & Christiansen (2008) described the cleat system as a system consisting of cubic matrix blocks. However, Nick et al., 1995 observed more complex structure systems which need to be characterised differently. A variety of cleat patterns in

Permian Queensland coals has been described (Pattison et al. 1996). Turner (2015) identified four groups of cleat morphologies based on CT-scans and core photographs (Figure 1b).

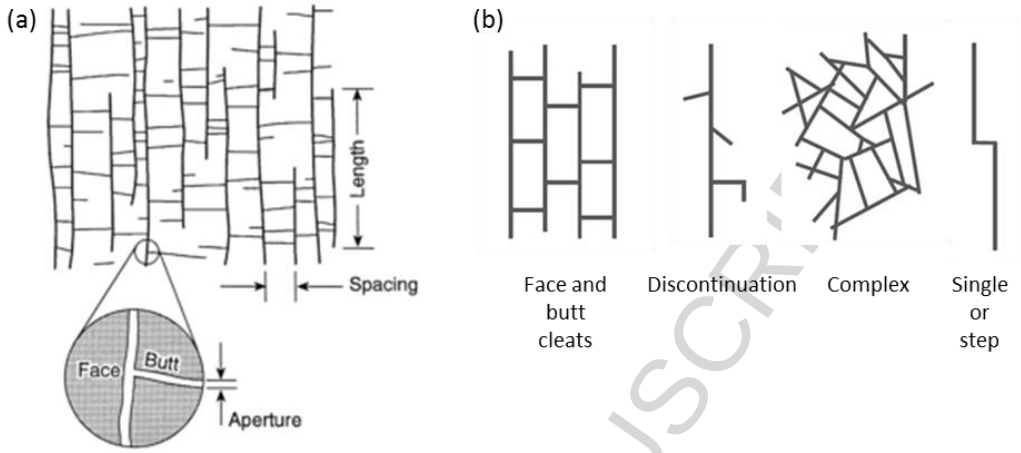

Figure 1 a. Schematics of orthogonal cleat system (Laubach et al., 1998), b. Cleat systems as described by Turner (2015)

Regardless of the cleat system, cleat geometry can be described as a function of frequency, aperture, size, the orientation both relative to other cleats and relative to in situ stresses, as well as the degree of their connectivity and porosity (Close 1993). Further, connectivity and spatial distribution of cleats, their cementation, filling and weathering influence geomechanical and hydraulic properties. In the subsurface, over geologic time, carbonate, quartz, or other cement may precipitate on the cleat walls, often disrupting connected networks. Cleat voids can contain organic materials, resin and authigenic minerals like clays, quartz and carbonates that can occlude or preserve fracture porosity (Laubach et al. 1998).

While for many coal fracture systems the porosity of fractures is found to be dependent on the stress field and therefore the depth (Barton et al., 1995), Laubach et al. (2004) showed that open fractures are not necessarily aligned or more permeable in certain directions relative to the stress field. In fact, the orientation of open natural fractures depends on the relative stiffness of the fracture and host material. Most of the coal measures in the East of Australia have little to no primary porosity. Approximately 75 % of eastern Australian coals current porosity is formed by a pore structure in the size range of meso- and micro-pores (< 50 nm) (Faiz & Aziz 1992).

1.2. *Relevance of cleat geometry measurements*

The term cleat refers to opening-mode fractures in coal beds. Besides cleat systems, the following literature review also covers fracture systems of other geo-materials. As a consequence, the terms cleat and fracture are used synonymously, with cleats referring to research done on the typical small scale structures in coal.

The aperture between fracture walls has been discussed as one of the main influencing parameters for flow in fractures. Fracture apertures cover a wide scale range as their variation is influenced by mechanical and chemical actions in the system (Bonnet et al. 2001). Philip et al. (2005) numerically investigated the effect of diagenesis on the initial flow properties of fracture systems, especially with respect to diagenetic effects on the connectivity of the fracture network. The results indicated that fracture permeability is more sensitive to fracture patterns and connectivity than aperture. The most commonly applied relation between aperture and permeability is the cubic law (Witherspoon et al. 1979). Long & Witherspoon (1985) claimed that fracture length and density are interrelated with flow rate. Networks with longer fracture lengths and lower fracture densities

exhibit higher connectivities and therefore higher permeabilities than those formed of shorter fracture lengths with higher densities.

The common approach for the modelling of fluid flow in fractures is to randomly generate artificial sets of fractures based on commonly known distributions (De Dreuzy et al., 2001). Galindo-Torres et al. (2015) examined randomly generated two-dimensional fracture networks and showed that the connectivity and conductivity of each individual fracture are related to the macro-conductivity and hence can be described by universal functions. The prediction of permeability is economically crucial as it determines whether commercial gas production rates can be achieved. Gas stored in coal seams (Clarkson & Bustin 2011), as well as groundwater in the system is transported through the cleats towards the producing wells (Scott 2002). Because seam permeability is a crucial factor for mine stability, minability, gas well performance and drainage behaviour, knowledge of cleat characteristics is essential for safe and efficient mining. The need for a better representation of fracture characteristics during permeability measurements has been pointed out by Huy et al. (2010). Further, the structure of cleat networks influences geomechanical behaviour like load bearing capacities of the seams and therefore impacts the mining process. The crucial role of the fracture system on the micro-scale requires, therefore, suitable image analysis tools allowing a streamlined and efficient, and yet comprehensive and differentiated characterisation of the fracture system.

1.3. *Cleat structure investigation by CT imaging*

While image processing has been widely used to describe structural properties of porous media (e.g. Vogel & Roth (2001), Khan et al. (2012)), literature on image processing methods for analysing cleat structure of coal samples is comparably sparse. Based on scanning electron microscopy of polished samples, aperture size distributions have been investigated and characterised by Karacan and Okandan (2000). Weniger et al. (2016) used images taken with optical microscopy of scanned polished sections to quantify cleat aperture, spacing, height, and frequency data and to derive permeability related to aperture and spacing based on the cubic law.

X-ray computed tomography (CT) scanning of coal samples as used in the presented study allows a non-destructive insight into a sample through the acquisition of projection images from three different directions. The interior of the sample is represented depending on their X-ray attenuation. By stacking slices of two-dimensional images, a three-dimensional data set is obtained. Coal matrix and pore spaces filled with air or liquid can be distinguished, as the X-ray attenuation is primarily a function of the energy, density and atomic number of the material (Ketcham & Iturrino 2005). Fractures and/or cleats and their variation of occurrence through the length of a cored coal sample can be detected and parameters like size, aperture and cleat connectivity can be quantified. Mazumder et al. (2006) used CT-scans to describe fracture orientations and cleat aperture and spacing in coal samples. The approach has been extended to deduce coal density and the distribution of inorganic material (Klawitter et al. 2013). Wolf et al. (2008) compared cleat angle distributions from drilling cutting to cleat orientation distributions from CT-scans from coal blocks of the same seams.

The presented paper aims at providing an image processing workflow to obtain geometrical properties of cleats in coal in a systematic way. CT scans are a useful tool for the testing and calibration of image and network-based models (Kumar et al., 2010). An innovative integrated application combining CT-scan based material characterization and process monitoring is promising to give an insight into the influence of heterogeneous rock properties like porosity, hydraulic conductivity and diffusivity on fluid transport processes and geomechanical properties (Cnudde & Boone, 2013). We are introducing an image processing based workflow to determine geometrical

parameters of coal cleats and discuss different cleat geometries. As shown by Laubach et al. (1998), face and butt cleats have different characteristics. We have developed a method that distinguishes face cleats and butt cleats by direction (Busse et al. 2015) and present detailed data for both cleat types. The results comprise cleat length, apertures, sizes, intensities, densities, shape parameter, spacing, orientation and connectivity. Therefore, the presented method provides more comprehensive information than previous cleat description approaches.

2. Sample material and methods

2.1. *Sample origin and preparation*

The coal samples used in this study were taken at the extension site of the Hail Creek Mine. The mine is situated on the East Coast of Australia, 120 km south-west of Mackay, Queensland, and is operated by Rio Tinto Coal Australia. Currently, sub-bituminous coal is extracted from two seams of the Rangal coal measures; the Elphinstone Seam, with an average thickness of 6.4 metres (m) and the Hynds Seam, averaging 8.3 m in thickness. Underlying are the Fort Cooper coal measures. They are extended along the north-western flank of the Hail Creek syncline (Clarke, 2007). The Elphinstone seam is made up of bright-banded coal that is interbedded with thin stone bands towards the bottom of the seam. The Hynds seam is intersected by a band of tuffaceous claystone which separates an upper layer of bright banded coals from dull banded coal in the lower half. The basal section of the Hynds seam is very dull, shaly coal interbedded with thin stone bands. With the present crucible swell numbers (CSN) larger than five both seams classify as hard coking coal. The vitrinite contents (Vitrinite %) in the Rangal coal measures are with percentages of 45 to 65 % lower in comparison to other coalfields in the Bowen Basin. The vitrinite reflectance (R_0Max) is the parameter used to determine the coal's rank. The older Hynds seam is a slightly higher ranked coal, with higher vitrinite levels, a more acidic ash chemistry and therefore higher coke strength after reaction (CSR). With its lower rank, the Elphinstone seam has higher fluidity. The maximum fluidity value is expressed in dial divisions per minute (MF (ddpm)). There is a decreasing trend in rank from south to north across the western margin for both seams. The Hynds seam has a feed ash content of around 25%, while for the Elphinstone seam it is around 20%. The Hynds seam on average yields 10% lower than the Elphinstone seam (Holwell 2007).

Three cored borehole samples taken normal to the bedding and from depths ranging between 141 m and 396 m are subject to this study: two of the Elphinstone (E1 and E2) and one of the Hynds seam (H1). After coring, the coal has been wrapped in plastic foil and duct tape, and was stored in a cool environment. Before scanning, the samples have been cut into smaller pieces, each approximately 6 centimeters (cm) in length. As a result of the sample handling the azimuthal orientation of the samples as found in-situ is unknown. Cleat directions, therefore, are only analysed relative to each other.

2.2. *Image Acquisition*

CT-Scans have been taken at a resolution of 53 micrometers (µm), with a size of 2048 by 2048 pixels, resulting after pre-processing in an image of 4.24 cm by 4.24 cm. The CT images were acquired using an Inveon Multimodality PET/CT system (Siemens) with the voltage of the X-ray source set to 80 kilovolts and the current to 500 microamps. The scans were performed using 360 degrees rotation with 360 rotation steps, a low magnification and a binning factor of 2. The exposure time was 800 milliseconds with an effective pixel size of 53.3 µm. The CT images were reconstructed using Cobra software (Siemens).

3. Analysis

3.1. *Image Processing*

An algorithm to extract geometric and topologic cleat information from a two-dimensional greyscale image has been developed and implemented in in the MATLAB® environment. The form definition of a cleat in a coal specimen is based on the widely accepted concept of an orthogonal network of butt and face cleats with both normal to the bedding plane (Figure 1). For the study of cleat occurrence and geometry in 2D image processing, a cleat has been defined as a feature that is longer than wide and aligned straight. Gaps in the direction of alignment are closed when they are smaller as the average cleat aperture in the region of interest.

The feature extraction and statistical analysis follow the workflow illustrated in Figure 2. The number of the section of this paper that discusses the respective topic is given on the right. It is to be noted that all results shown in the following are given in mm based on the fact that each square pixel has a side length of 53 µm. Sample E2 which exhibits a network of face and butt cleats is used to demonstrate the details of the image processing steps. The image processing results for this sample, as well as for two other samples are presented in section 4.

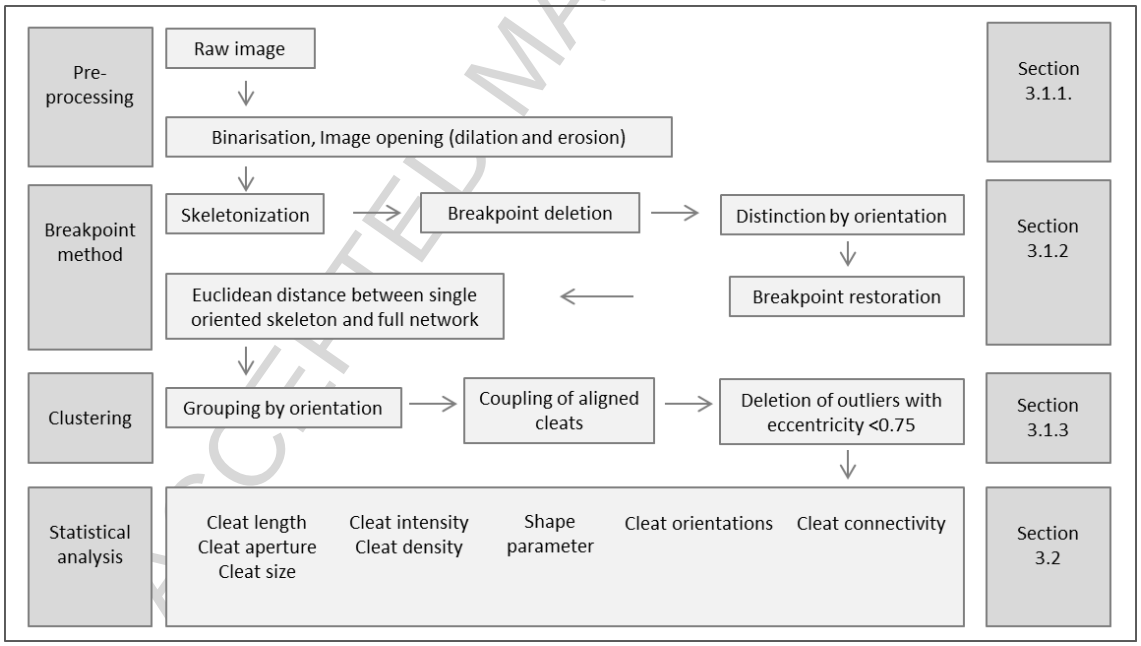

Figure 2 Workflow of image processing

3.1.1. Pre-processing

The scanning results in image files from three directions: axial, sagittal and coronal planes (Figure 3). The cleat system in Sample E2 is orthogonal to the bedding planes and the axial view with the axial plane parallel to the bedding planes of the coal sample was chosen for this 2-dimensional study to best capture the cleat structure within a single image (Figure 4a). The image was cropped to reduce the image size and to remove the outer rim of the sample image. This way, any possible disturbance due to sample handling and preparation can be reduced (Figure 4b). The initial image size before cropping is 2048 x 2048 pixels; afterwards, the dimensions are reduced to 800 x 800 pixels, showing an image region of 4.24 x 4.24 cm^2.

The distinction between face and butt cleats in each image is made visually based on the concept by Laubach et al. (1998). Face cleats are dominant and perpendicular to the bedding plane. The fewer orthogonal butt cleats generally terminate when they encounter face cleats. Based on this commonly used description, the positively orientated structures (relative to the x-axis of the image) detected in the image represent face cleats, the negatively orientated structures are considered to be butt cleats.

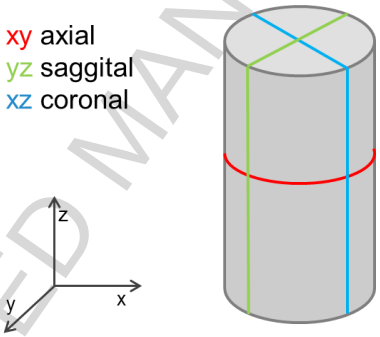

Figure 3 Axial, sagittal and coronal planes of the sample

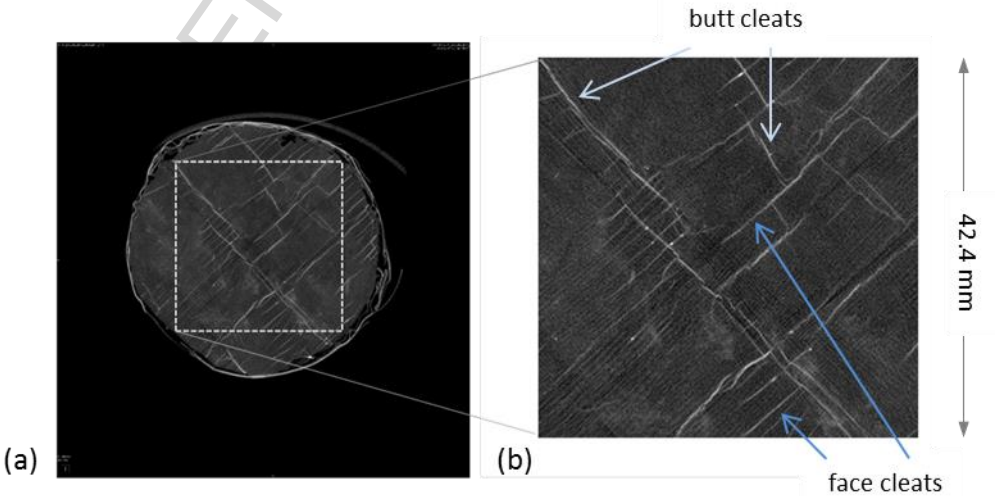

Figure 4 a. CT-scan image and b. chosen region of interest of sample E2

The grayscale values of the cropped image are displayed in Figure 5a. Segmentation processes help to reduce the information content of images to the features relevant to answer the considered questions. To facilitate the distinction of features in an image, greyscale contrasts can be adjusted, using thresholds fitted to the relative problem. Particularly helpful and widely used is a binarisation of the image based on a certain threshold on its greyscale (Gonzales et al., 2004). A greyscale image is turned into a binary image by choosing a grey level in the original image as threshold and turning every pixel value into black or white depending on their relative position to the threshold. The

binarisation threshold is chosen based on the distribution of the grayscale values. The grayscale values usually distribute uni-modally. Therefore, the Rosin threshold to distinguish between the present cleats and the matrix (Rosin 2001) is chosen. Using this method, a straight line is drawn between the histogram peak and the maximum occurring value (Figure 5a). The threshold is selected at the point of the histogram that is furthest from the straight line. The threshold value obtained for sample E5 greyscale image is 92 out of the 255 grayscale values, which equals a grayscale ratio of 0.36. The resulting binarisation of the E2 greyscale image is shown in Figure 5b. In this case, white pixels may provide information on the cleat structure and black pixels can be considered as coal matrix.

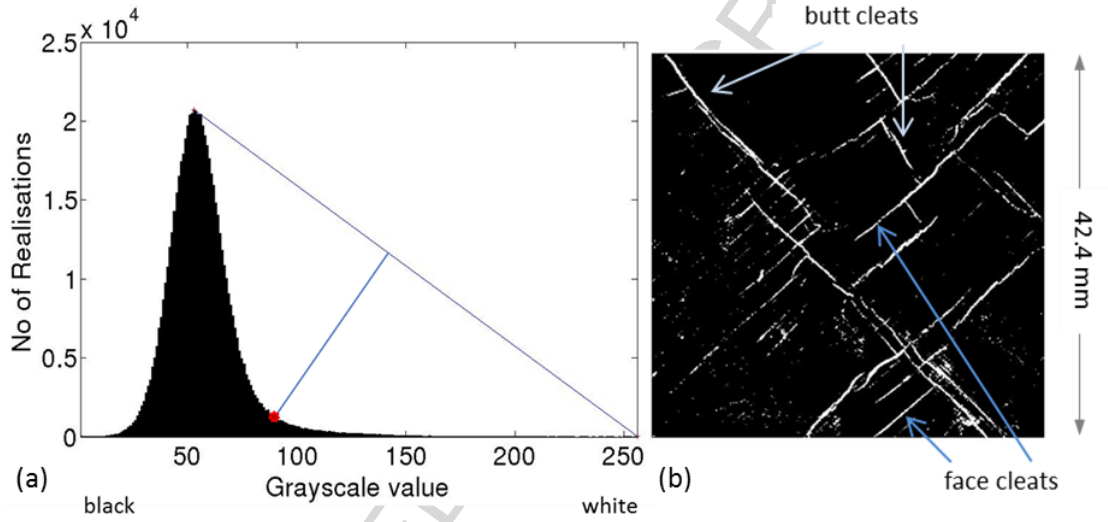

Figure 5 a. Plot of grayscale distribution with threshold (red dot) identified using the definition by Rosin (2001) and b. resulting binarised greyscale image of sample E2

Once binarised, the black and white images allow for a simple feature extraction and further processing, e.g., logical operations, feature connection through erosion and dilation, skeletonisation and edge detection (Gonzales et al. 2004). Single pixels or small pixel clusters in a binary image are frequently considered as noise and are removed by digital noise filtering. However, filtering was not applied in this case, since it may also partially remove those small clusters that line up perfectly with other features and that, as a result, represent part of a cleat. Dilation and erosion serves to reconnect features that might have been divided during the image acquisition and processing. In the dilation stage the features are thickened with pixels added onto the outside in the form of a defined disk-shaped structuring element with a certain radius. The erosion uses the same filter to delete the outer edge of pixels, with the exemption of the pixels now connecting two features (Figure 6). The result of the dilation and erosion on the image of the cleat structure subject to this study is shown in Figure 7.

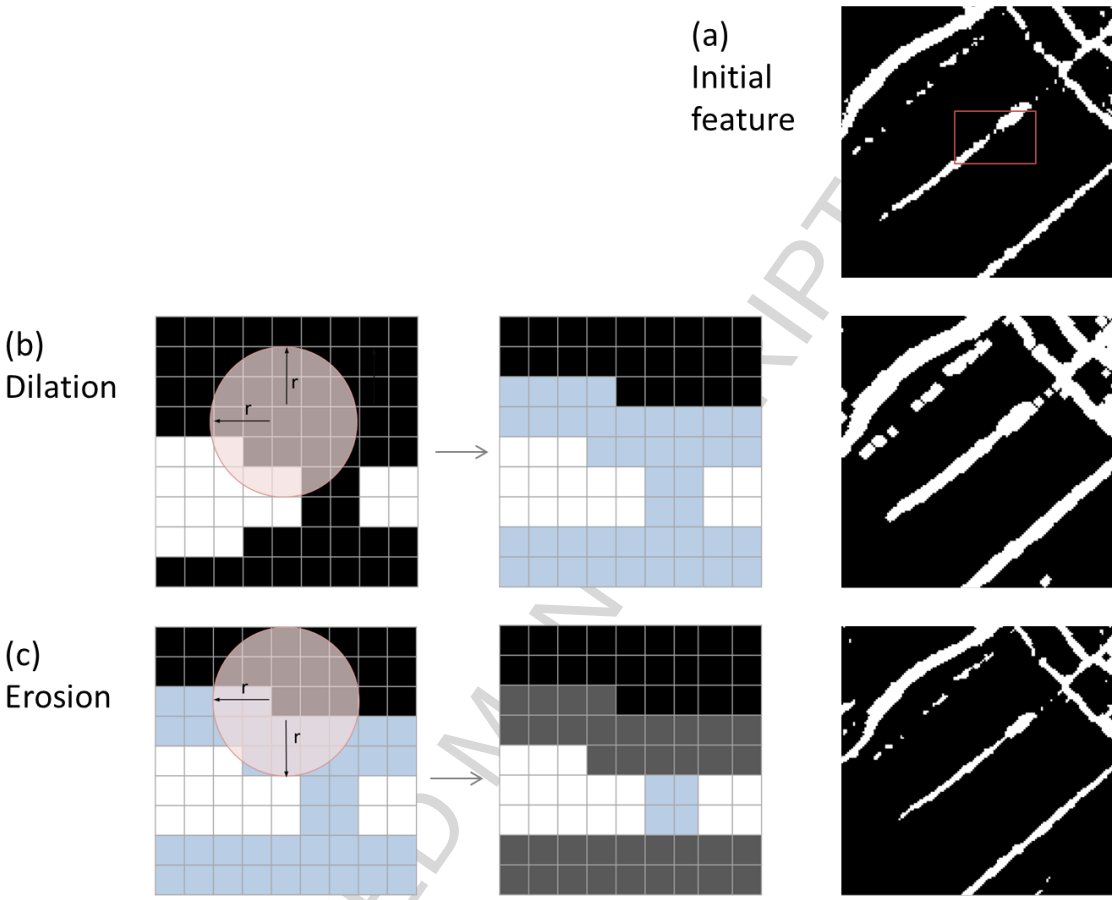

Figure 6 a. Initial feature and the principle of b. dilation and c. erosion of image features using a disk-shaped element with radius r to reconnect features originally being separated due to the binary process

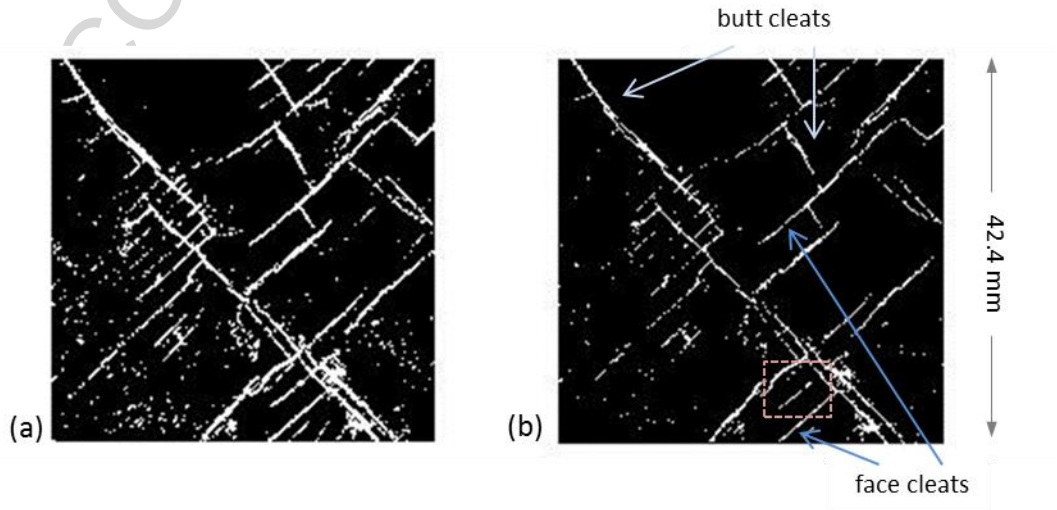

Figure 7 a. Dilated and b. eroded binary image of sample E2. The marked area in b is shown in Figure 8.

3.1.2. Breakpoint method for cleat detection

To extract features that represent the cleats based on the cleat definition made earlier, the following steps are done on the pre-processed picture. Firstly, the skeleton of each of the features are displayed and their breakpoints are calculated. Skeletonisation helps to visualise shape properties. In the process, a feature is minimised to its skeleton, i.e. its midline (Figure 8). The skeleton illustrates topological as well as geometrical shape properties as length and direction. In the skeleton, pixels with only a single touching neighbour are representing end points, pixels with more than two neighbours are breakpoints (Pratt 2001).

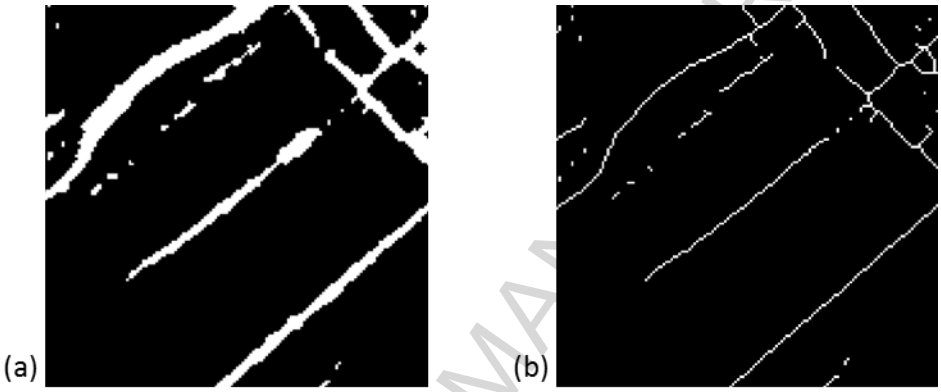

Figure 8 Inset of Figure 7b with a. features and b. skeletons of the features of sample E2

Breakpoints mark a crossing between or a joint of two skeletons. These breakpoints are removed from the binary image to get a set of aligned skeleton sections (Figure 9). Using the MATLAB image processing toolbox ('regionprops') the orientations of the skeletons are calculated. Due to the nature of coal cleats being perpendicular to each other, the distinction between face and butt cleats can be done (Figure 10). Once this distinction is done, the skeleton sections are bridged by filling the breakpoints back into the image. The result is the full skeleton of each cleat. Cleats are by definition relatively straight features with no discontinuation.

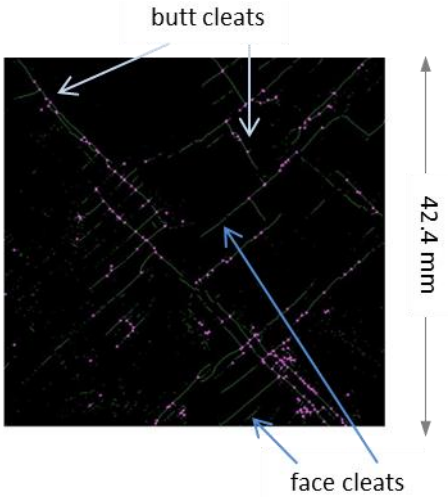

Figure 9 Skeletons and breakpoints of the features in the binary image of sample E2

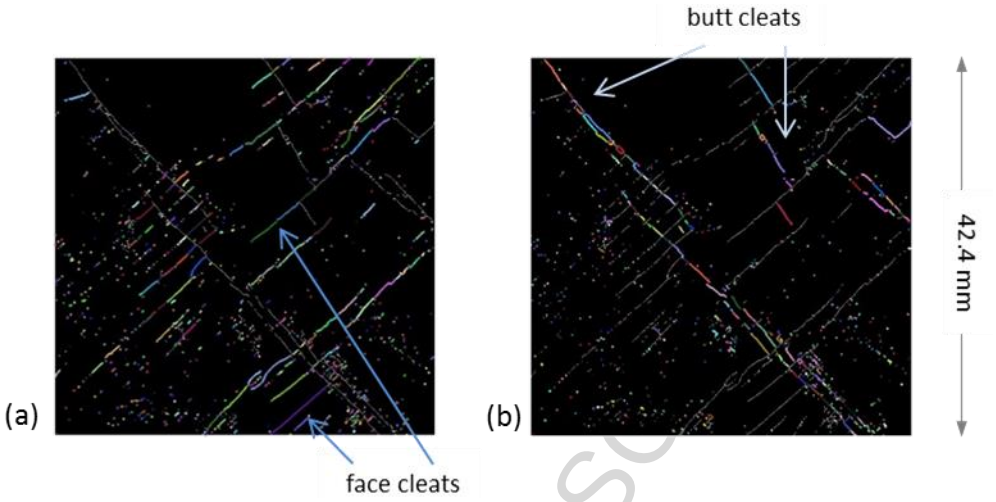

Figure 10 Distinction of skeleton sections based on orientation, a. face cleats and b. butt cleats. Each individual skeleton section is identified by a different colour in the binary image of sample E2

To get the complete set of shape parameters of the features, the skeletons are overlapped with the inverse of the original binary cleat network using a Euclidean distance function. Face and butt cleats are reconstructed around the skeletons based on the input cleat network. The fitting is done using visual trial and error (Figure 11). Based on the Euclidean distance one can determine the distance from each cell to the closest non-zero element (Deza & Deza 2009). For Cartesian coordinates, the Euclidean distance between two points a and b in a n-dimensional space is calculated by

$$ED(a,b) = ED(b,a) = \sqrt{\sum_{i=1}^{n}(b_i - a_i)^2} \quad (1)$$

In Figure 11a and Figure 11b the original binary image (green) is masked with the face and butt cleat features that have been extracted (red). Finally, the reconnected features that represent face and butt cleats are extracted (Figure 12a and Figure 12b) which can be used to calculate individual feature properties.

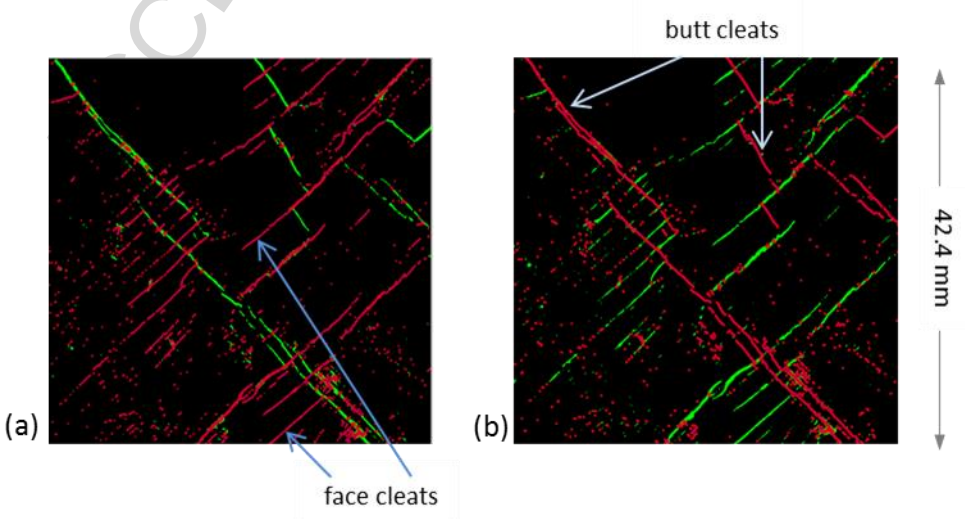

Figure 11 Overlap of the original binary image (green) with the extracted, reconnected and grouped features (red) for a. butt cleat and b. face cleat orientation of sample E2

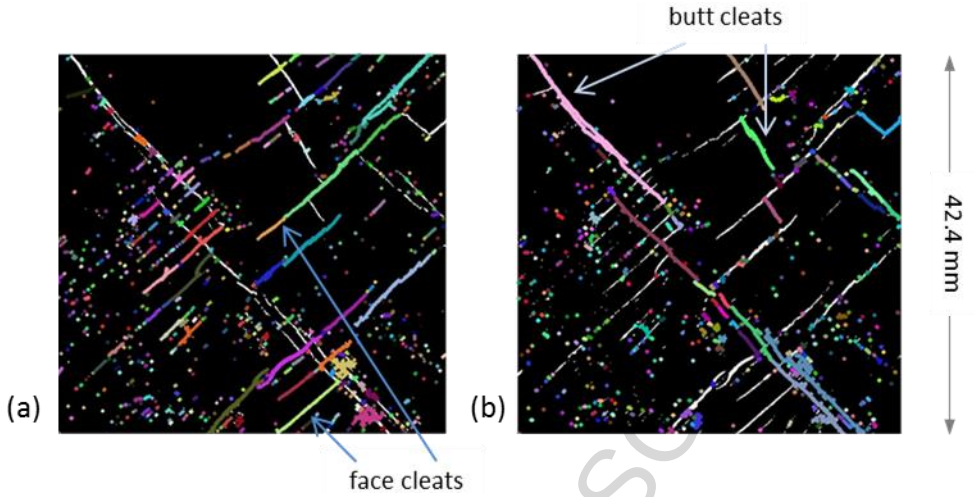

Figure 12 Reconnected features present for both a. face cleat and b. butt cleat orientations of sample E2

3.1.3. Clustering of reconnected features

A feature in a grey scale image representing a cleat has been defined by the pixel's greyscale values exceeding a defined threshold value and the shape being a cluster of aligned pixels that is longer than wide. To fulfill the latter part of the definition, the features are grouped based on their eccentricity, orientation, and position. Eccentricity is deduced by fitting a major and minor axis to each feature and defined as the ratio of the distance between the foci of the ellipse and its major axis length. The principles of major and minor axis length, perimeter and area size are presented in Figure 13. The ellipse fitting is based on an ellipse perimeter that has the same normalized second central moment (variance) as the area of a feature. The features that have an eccentricity below 0.75 are not considered as cleats. Eccentricity takes values between 0 and 1, with 0 representing a circle, and 1 a line shape (Figure 14).

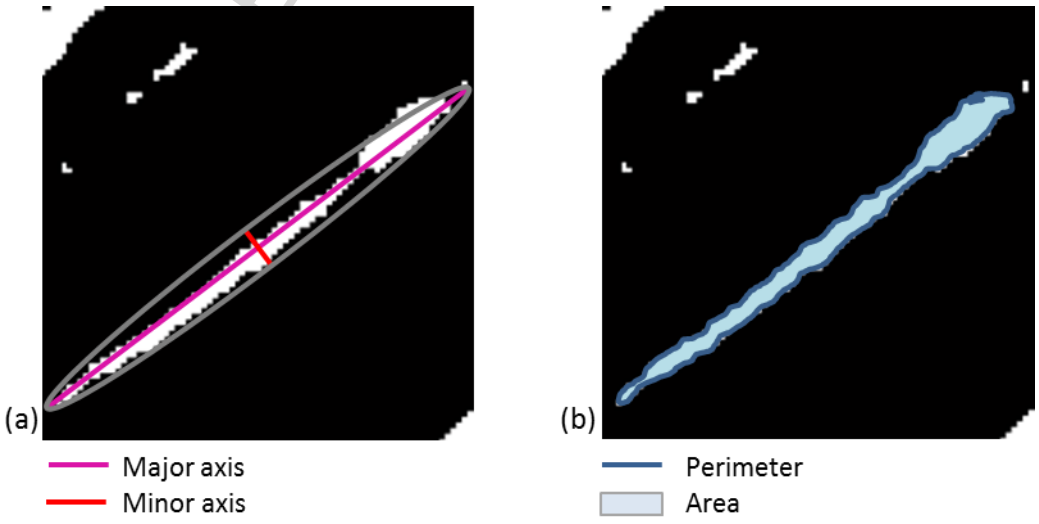

Figure 13 Principle of shape parameters used in the study, a. ellipse perimeter that has the same normalized second central moment (variance) as b. the area of a binary image feature

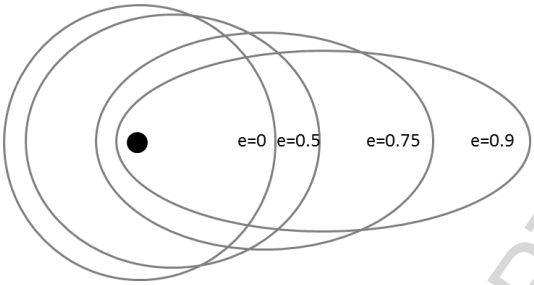

Figure 14 Principle of eccentricity (after http://earthobservatory.nasa.gov)

In the next step, gaps between the line-shaped features (those with an eccentricity larger than 0.75) are bridged. Line-shaped features that are aligned along the same axis with a gap between them that is smaller than the average cleat aperture occurring in the image are grouped to one cleat. A line-shaped structuring element with the length of the average aperture is used to fill the gap in the respective direction in an image opening process (dilation and erosion). At this stage, clusters that consist of less than 20 pixels are removed in a final filtering process. As a result of the image processing and clustering two sets of extracted reconnected features are obtained that represent cleats: a set of face and a set of butt cleats. They are pictured in Figure 15a and 15b.

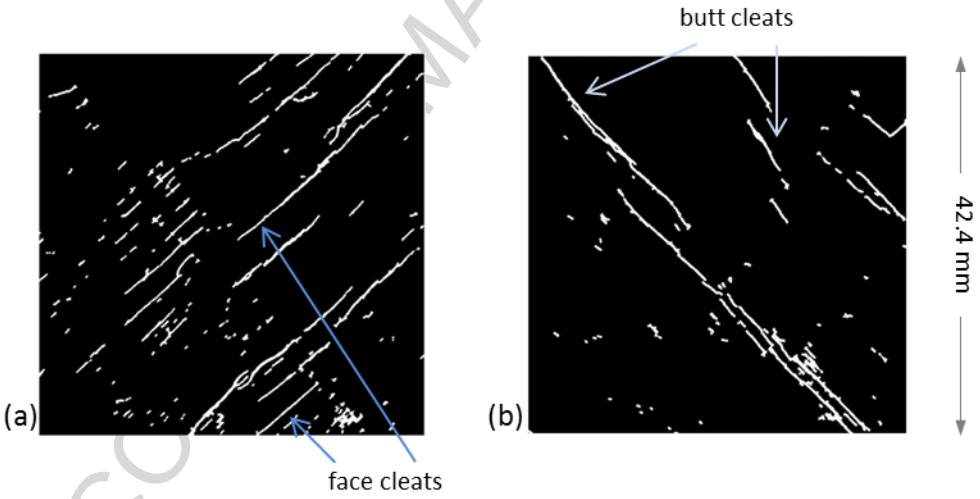

Figure 15 Extracted reconnected features that represent a. face cleats and b. butt cleats of sample E2

3.2. *Statistical analysis of cleat properties*

The extracted, reconnected line-shaped features can be considered as a close approximation of the shape of cleats in the CT-scan images of coal samples and are referred to as cleats throughout the remainder of this paper. Using the image processing toolbox of MATLAB, geometric properties of all cleats are measured and a range of shape parameters are obtained. Feature specific image properties are sizes like cleat length, apertures, and total size distributions. Further, intensity and density, shape parameter and cleat spacing are measured. Relative orientations are given where a network of face and butt cleats is present. The connectivity of the cleat network is described by the Euler characteristic and the density of intersections. Distributions of cleat properties are both shown in histograms and log-log plots that are fitted with the power law function that describes the distribution. In the log-log plots the centre of the bins that have been selected are displayed as a point value.

3.2.1. Cleat length, aperture and size distribution

Cleat length is a critical property for network connectivity and therefore strongly influences mechanical properties and flow behaviour in the system (Galindo-Torres et al. 2015). The characteristics of fracture length distribution are required as an input to discrete fracture networks to model physical properties of fractured rocks (Chilès (2005), Ghaffari et al. (2011)). This parameter typically has been found to follow a truncated power law distribution with a tall head and a long tail by Walsh & Watterson 1993. A power law distribution has the general form

$$n(w) = i\, w^{-c} \quad (2)$$

With n being the number of occurrences of the fracture property w, i being a coefficient of proportionality and c the power law exponent referred to as the fractal dimension.

Others (e.g. Rouleau & Gale (1985)) have used a lognormal distribution to describe fracture length distributions. The lognormal distribution is given by

$$n(w) = \frac{1}{w\sigma\sqrt{2\pi}} exp^{-\left(\frac{\ln w - \mu^2}{2\sigma^2}\right)} \quad (3)$$

With the μ being the logarithmic mean and σ the standard deviation of the fracture property w. Further, for non-parallel fractures the total length in the region is an indicator of connectivity (Dershowitz 1984). Cleat lengths extracted from the image are based on the major axis length of the extracted line-shaped features.

Compared to studies on fracture length, there are relatively few studies on the distributions of the aperture. Aperture has been found by Bonnet et al. (2001) to follow a gamma law distribution; that is a power law with an exponential tail. Madadi & Sahimi (2003) approximated the distribution of fracture apertures in a rock by log-normal distributions. Weniger et al. (2016) measured a maximum aperture of 2 mm, and a minimum of 2 µm at the limit of resolution in their study. The median aperture was 29 µm. In this study, cleat apertures extracted from the image are based on the minor axis length.While fracture size often refers to length and height (e.g. Hooker et al. (2013)), it is defined as the area of the fracture face (length and aperture) for the present two-dimensional study. Fracture-size distributions have been found to either being centred onto a specific value with fewer smaller or larger values present (Priest & Hudson 1976) or are scale-independent for example in power-law size distributions (Ortega et al., 2006).

3.2.2. Cleat intensity and density

In the presented two-dimensional case the total number of cleats, cleat intensity and density are useful measures to characterize the cleat system (Dershowitz 1984). The intensity of cleats is calculated as the sum of the cleat area over the whole image area. It is, therefore, dimensionless. The density is defined as the total number of cleats in the image area.

$$intensity = \frac{cleat\ area}{sample\ area}\ [-] \quad (4)$$

$$density\ = \frac{nr\ of\ cleats}{sample\ area}\ [mm^{-2}] \quad (5)$$

3.2.3. Cleat shape

A useful shape parameter is the ratio of aperture to length.

$$\frac{aperture}{length}\ [-] \quad (6)$$

The relation between fracture aperture b and length l has been proposed to follow

$$b = il^c \quad (7)$$

with i being a constant and c varying between 0.5 and 2 (Bonnet et al. 2001).

3.2.4. Cleat spacing

The distribution of cleats is highly variable with intensely fractured bands and less intensely fractured bands. This distribution is captured by the measure of the spacing between the fractures. Characteristic sizes of cleat spacings are between 10 – 25 mm (Wang et al., 2009). Dawson and Esterle (2010) found that for specific vitrain layers, the cleats could be spaced as closely as less than a millimetre apart. Further, the spacing of the cleats tended to be proportional to fracture size for given types of cleats. For example, a vitrain layer that confined smaller cleats, as well as larger master cleats which traversed multiple coal layers have been observed.

The perpendicular spacing between the cleats in the region of interest is determined and average cleat spacing for both orientations is calculated. Following the principle of scanline mapping based on Acoustic Televiewer and Optical Televiewer logs, that is used in the field (Jing & Stephansson 2007), a grid perpendicular to the main features in the image is constructed (Figure 16). It consists of a total number of 31 gridlines in the diagonal case and 17 gridlines in the vertical case with a distance of each 2.65 mm between the lines. The distance between features along the gridlines is measured.

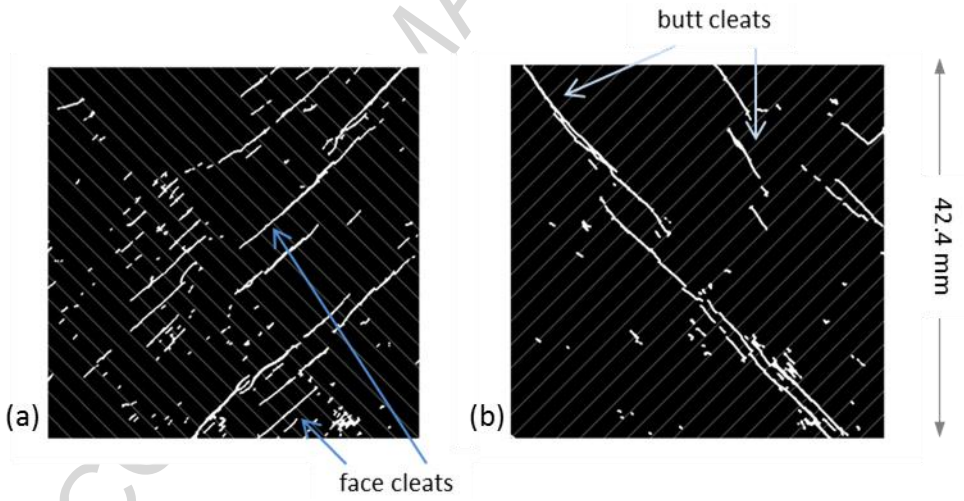

Figure 16 Spacing measurements along grid with 2.65 mm distance for a. face and b. butt cleats

Quantitative statements of spacing are only meaningful with a scale reference included in the analysis and the method that has been used to measure cleat spacing. Laubach et al. (1998) plotted cleat spacings that represent the averages of all measured spacings having a specific aperture measurement and found cleat spacing to increase linearly with cleat aperture that spanned a particular fractured bed. In the presented case study the average of spacing and apertures along the gridlines that are shown in Figure 16 are used. An illustration of a representative gridline is shown in Figure 17.

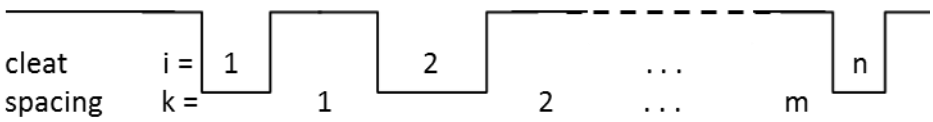

Figure 17 Cleats and spacings along gridline

For a representative gridline with a number of cleats i of a certain aperture and k spacings of a certain length the following relationships have been established:

$$avg\ spacing = s_{avg} = \frac{\sum_{k=1}^{m} spacing}{\sum_{i=1}^{n-1} nr\ of\ cleats} \quad (8)$$

$$avg\ aperture = \mathrm{b}_{avg} \frac{\sum_{i=1}^{n} aperture}{\sum_{i=1}^{n} nr\ of\ cleats} \quad (9)$$

Displaying the average spacing s_{avg} against the average aperture b_{avg} in a log-log plot, a power law can be fitted that follows the following form

$$s_{avg} = i\ {b_{avg}}^{-c} \quad (10)$$

With i being a coefficient of proportionality and c the power law exponent referred to as the fractal dimension (Laubach et al. 1998).

As an average over the sum of the number of gridlines g in the image, the gridline frequency is defined as

$$gridline\ frequency = \frac{\sum_{1}^{g} nr\ of\ cleats\ along\ gridlines}{\sum_{1}^{g} gridline\ length}\ [mm^{-1}] \quad (11)$$

3.2.5. Cleat orientations

Cleat orientations are illustrated using rose plot diagrams. The orientation of each cleat is calculated as the angle from the x-axis of the input image and displayed in fractions of 360 degrees. To illustrate length differences between face and butt cleats, the cleats are weighted by their length in mm. For example, a cleat of 10 mm length is counted ten times, a 5 mm long one five times. The cleat orientations show relative orientations of face and butt cleats to each other. The plot is therefore only made for samples where face and butt cleats are present.

3.2.6. Cleat connectivity

Long & Witherspoon (1985) show that the degree of interconnection and therefore permeability increases as fracture length increase and densities decrease. Using image processing methods, structural connectivity of features can be described using the Euler characteristic. In 2D the Euler characteristic is the total number of features C in the image minus the total number of holes H in those features.

$$E = C - H \quad (12)$$

For a network in which at least one path exists between any two nodes, the maximum number of branches that could be removed without breaking the network into parts is 1 - N. Breaking a single connection increases the Euler characteristic by 1, the addition of a connection decreases it by 1. In other words: the Euler characteristic is a measure of how many connections in a structure can be severed before the structure falls into two separate pieces (Odgaard & Gundersen 1993). Therefore, depending on the material of interest, a highly connected structure has a negative Euler characteristic of up to several thousand in a volume of 1 cm^3.

Next to the total length of fractures in the region of interest, the density of fracture intersections is a measure for connectivity of a system (Jing & Stephansson 2007). It is defined as the number of fracture intersections per unit area. It is derived using the number of breakpoints (Figure 9) and the image area

$$density\ of\ cleat\ intersections = \frac{nr\ of\ cleat\ intersections}{image\ area}\ [mm^{-2}] \quad (13)$$

4. Results

Characteristics of coal cleat networks have been extracted based on the image processing method presented in the Analysis chapter. Three coal samples have been analysed; the results are

summarised in the following. The cleats captured in the images are mineralised, which makes them well visible in the scans. Cleat mineralogy in this set of samples comprises of kaolinite, calcite, and traces of anastase.

4.1. *Sample origin and cleat geometry*

Sample E1. Core sample E1 is of 6.22 cm length and was taken from the Elphinstone seam at a depth of 163.72 to 163.78 m. The image with an area of 1797.76 mm^2 refers to an in-situ depth of 163.76 m. Three sets of cleats have been extracted: face cleats I, face cleats II and butt cleats (Figure 18).

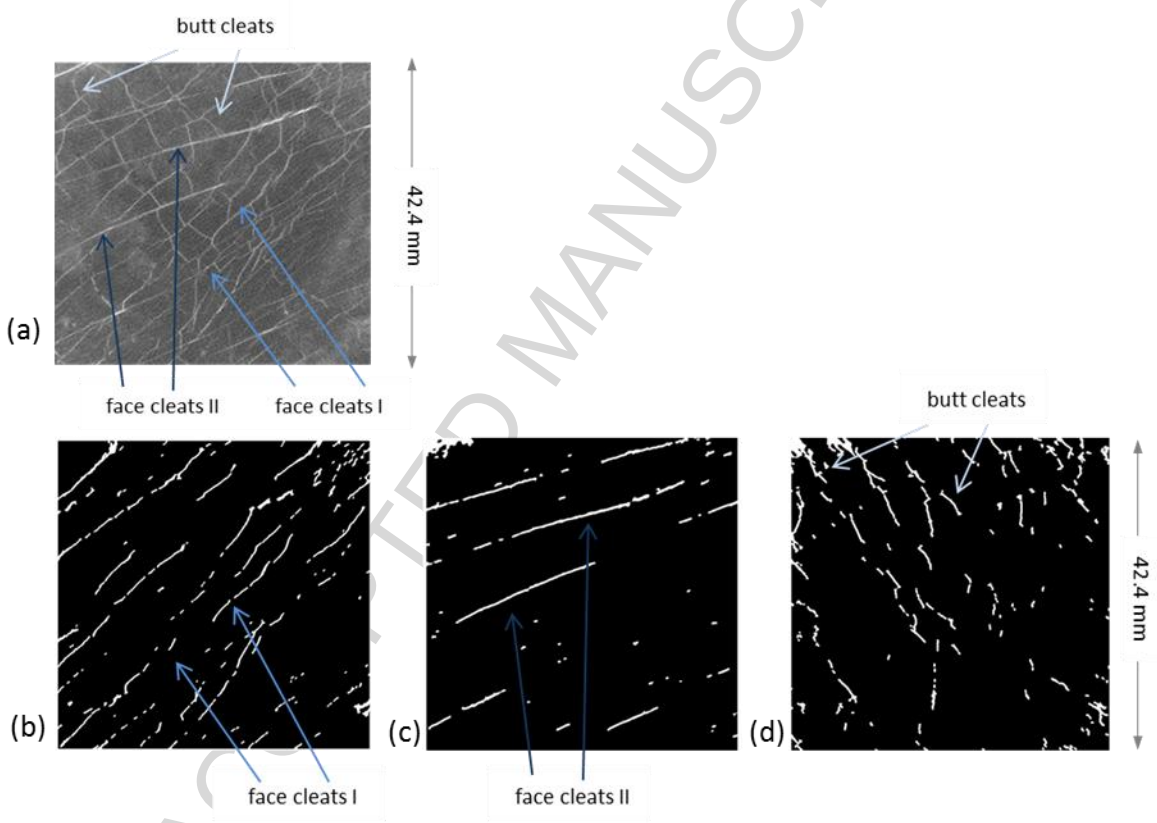

Figure 18 a.CT scan of sample E1 and binary image of b. face cleats c. face cleats II and d. butt cleats after segmentation

Sample E2. Sample number E2 was taken at the Elphinstone seam. The scanned sample is of 7.5 cm length and was taken at a depth of 290.79 to 290.865. The image with an area of 1797.76 mm^2 refers to an in-situ depth of 290.8 m. The image processing workflow has been introduced using this example. Face cleats and butt cleats are present (Figure 19).

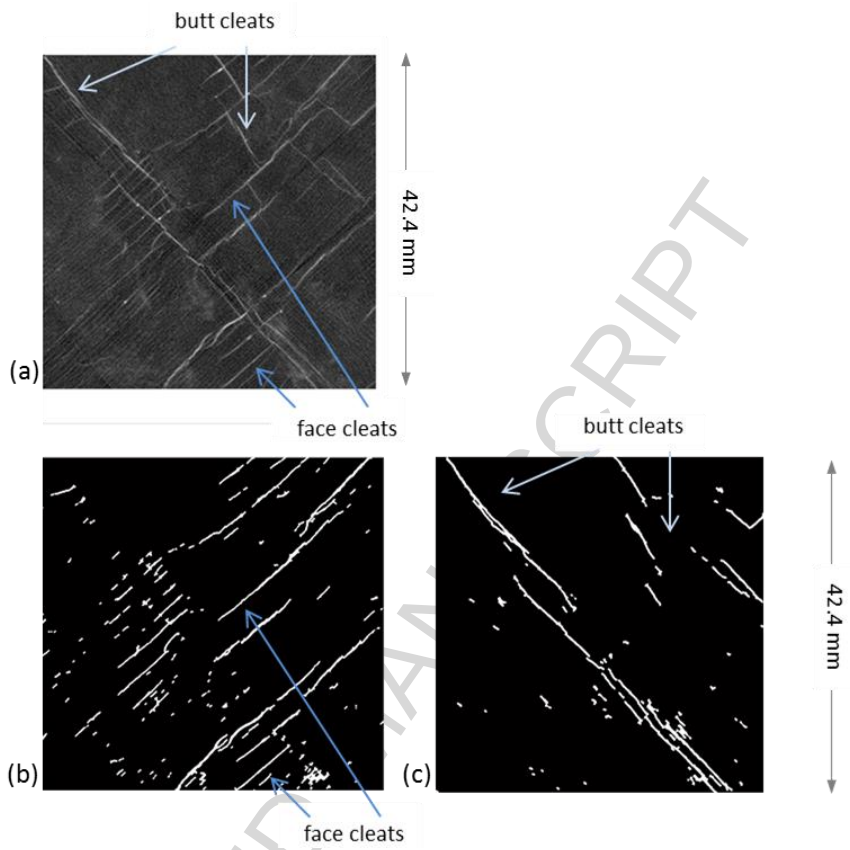

Figure 19 a. CT scan of sample E2 and binary image of b. face cleats and c. butt cleats after segmentation

Sample H1. Sample number H1 was taken at the Hynds seam. The scanned sample is of 7.45 cm length and was taken at a depth of 361.66 m to 361.74 m. The image with an area of 1797.76 mm^2 refers to an in-situ depth of 361.69 m. In this sample parallel face cleats, but no butt cleats are visible (Figure 20).

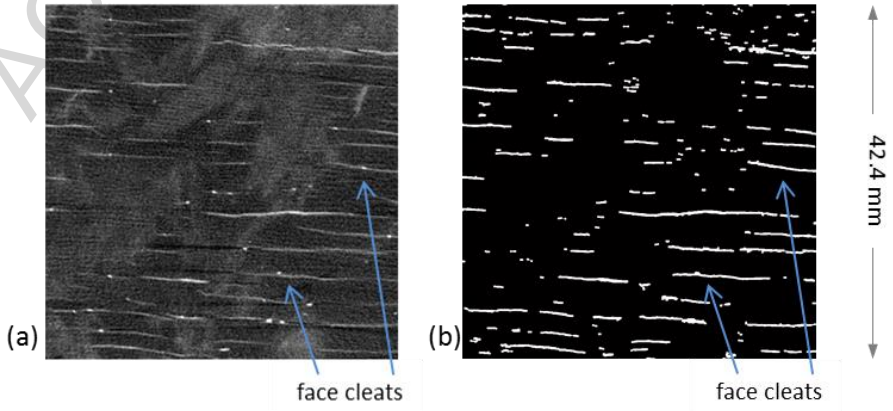

Figure 20 a. CT scan of sample H1 and b. binary image of face cleats after segmentation

4.2. *Cleat length, aperture and size distribution*

Sample E1. The total number face cleats I is 149; of face cleats II 56, the total number of butt cleats is 123. The total face cleat I length sums up to 308.24 mm, for face cleats II to 152.53 mm, for

butt cleats 230.17 mm. Cleat length distribution follows a power law (Figure 21a). The distributions of the face cleats I and the butt cleats are similar. Cleat apertures (Figure 21b) are following power law distributions. The total area size of butt cleats in the image is 74.69 mm^2, the face cleats I take up 69.03 mm^2, face cleats II 49.37 mm^2. A power law distribution is fitted to all three cleat sets, as can be seen in Figure 21c.

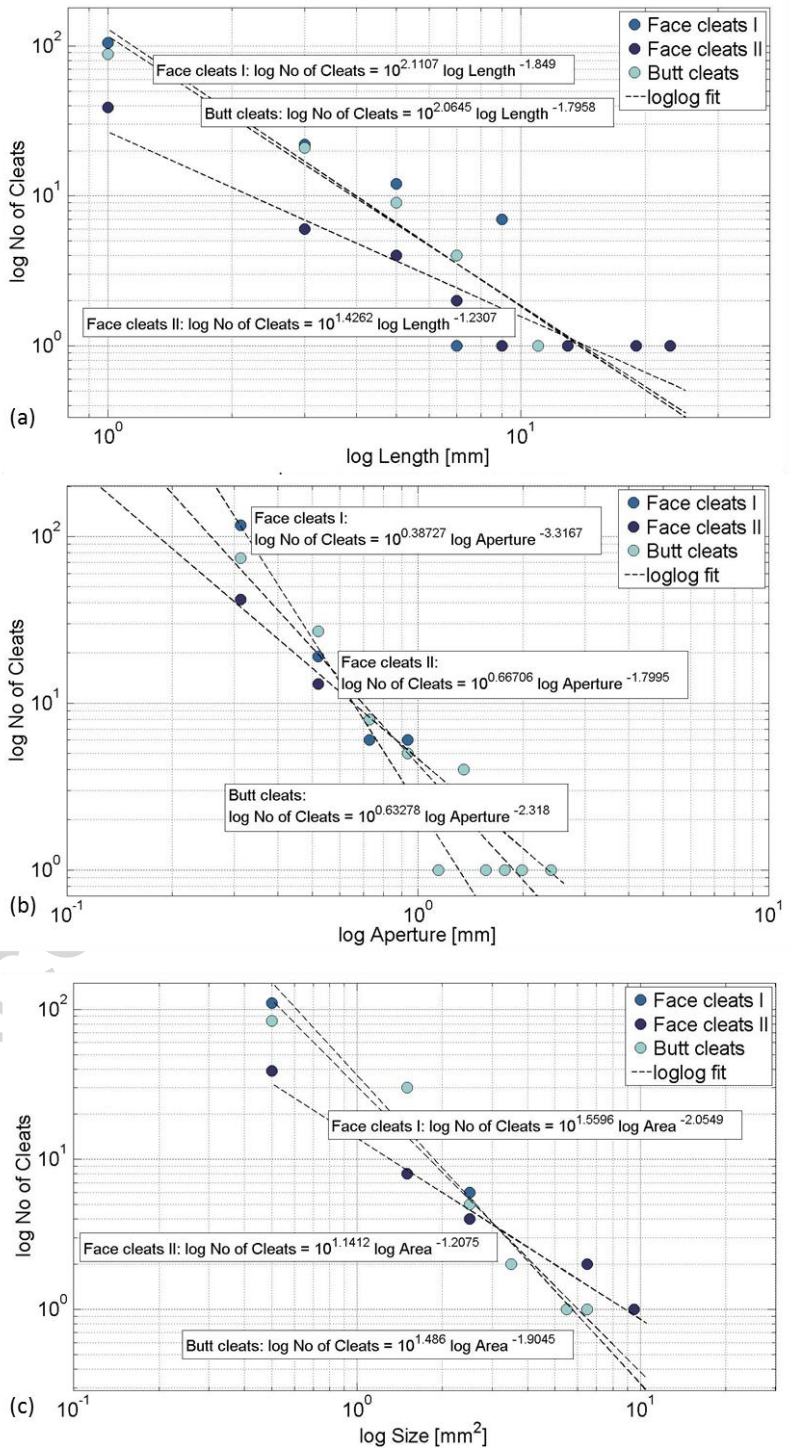

Figure 21 log-log plot of a. Length distribution, b. Aperture distribution, c. Size distribution of sample E1

Sample E2. The total number face cleats is 139; the total number of butt cleats is 60. The total face cleat length sums up to 311.19 mm, for butt cleats to 179.7 mm. The cleat length distribution follows a power law distribution (Figure 22a). Looking at the distributions of the aperture, they follow a power law distribution for both cleat types (Figure 22b). The total area size of butt cleats in the image is 56.08 mm^2, the face cleats take up 74.90 mm^2. The cleat size distributions are shown in Figure 22c.

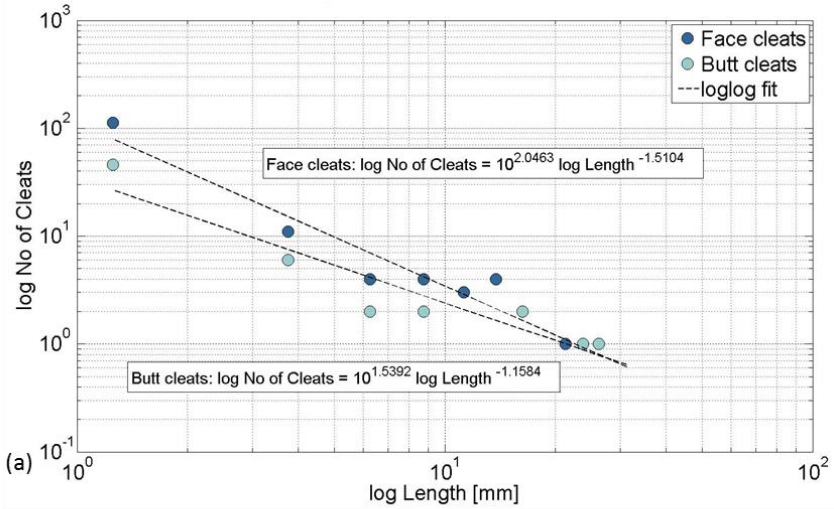

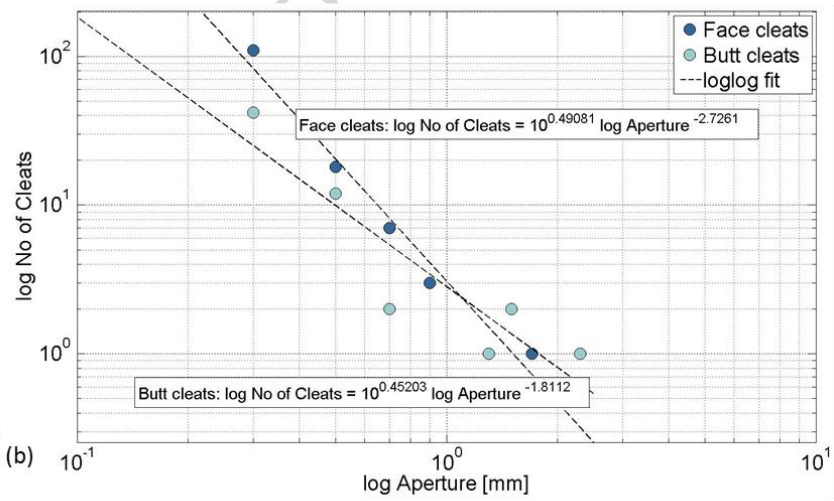

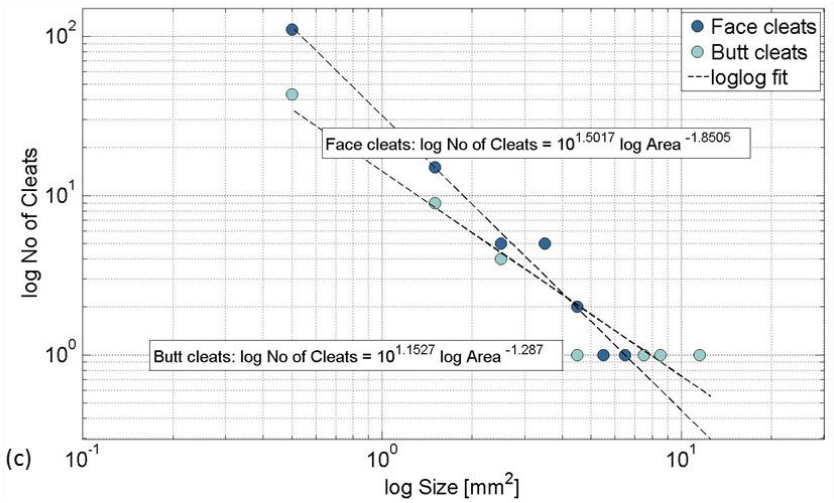

Figure 22 log-log plot of a. Length distribution, b. Aperture distribution, c. Size distribution of sample E2

Sample H1. The total number of the face cleats is 172. The total face cleat length sums up to 412.26 mm. Cleat length distribution can be fitted to a power law distribution (Figure 23a). The aperture of the face cleats in sample H1 follows a power law distribution that is shown in the plot in Figure 23b. The total area size of face cleats in the image is 103.67 mm^2. The cleat size distribution follows a power law distribution (Figure 23c).

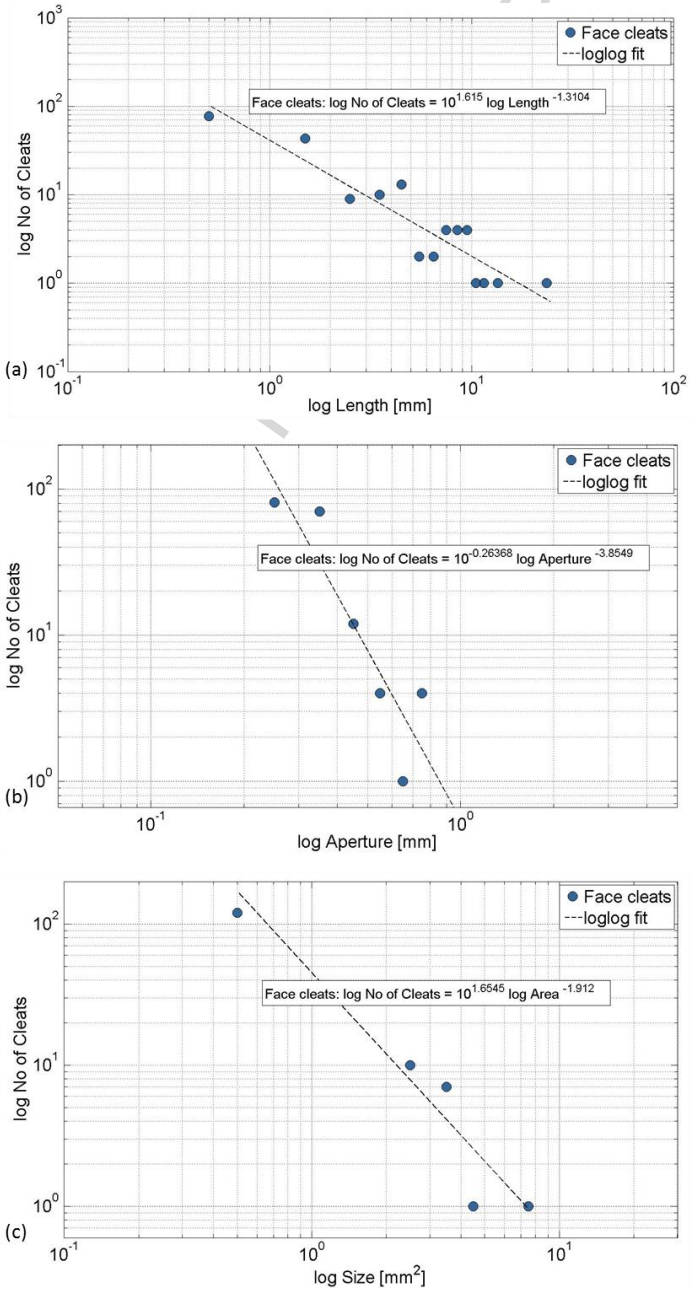

Figure 23 log-log plot of a. Length distribution, b. Aperture distribution, c. size distribution of sample H1

4.3. *Cleat intensity and density*

Cleat intensity and density Sample E1

Sample E1. The cleat intensity for face cleats I is 0.038, for face cleats II 0.028 and for the butt cleats 0.042. Cleat density for face cleats I is 0.083 mm^{-2}, for face cleats II 0.032 mm^{-2} and for butt cleats 0.068 mm^{-2}.

Sample E2. Cleat intensity measured for the face cleats is 0.0417, for the butt cleats it is 0.0312. The cleat density of the face cleats is 0.077 mm^{-2} and 0.0334 mm^{-2} for the butt cleats.

Sample H1. The cleat intensity of the face cleats is 0.058, their cleat density 0.096 mm^{-2}.

4.4. *Cleat shape*

Sample E1. The cleat shape parameter for the cleats extracted from sample E1 is shown in Figure 24.

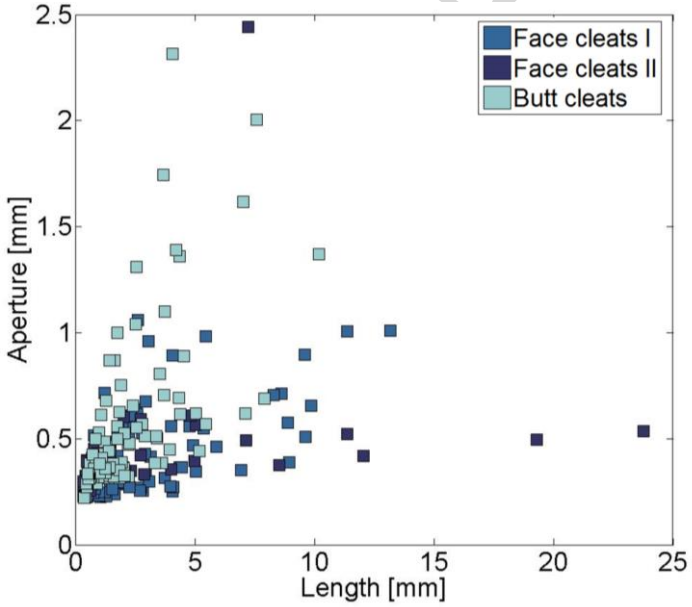

Figure 24 Aperture / length ratio sample E1

Sample E. The shape parameters of the sample E2 is shown in Figure 25.

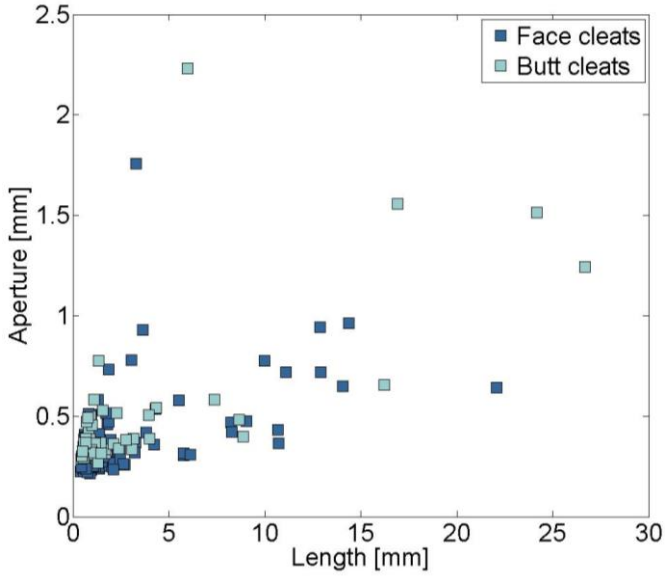

Figure 25 Aperture / length ratio sample E2

Sample H1. The ratio of aperture and length, as well as the ratio of perimeter and area, are shown in Figure 26. The aperture vs. length plot shows two main directions of the distributions with some of the very short cleats having longer apertures than average and another set of cleats having larger apertures with increasing lengths.

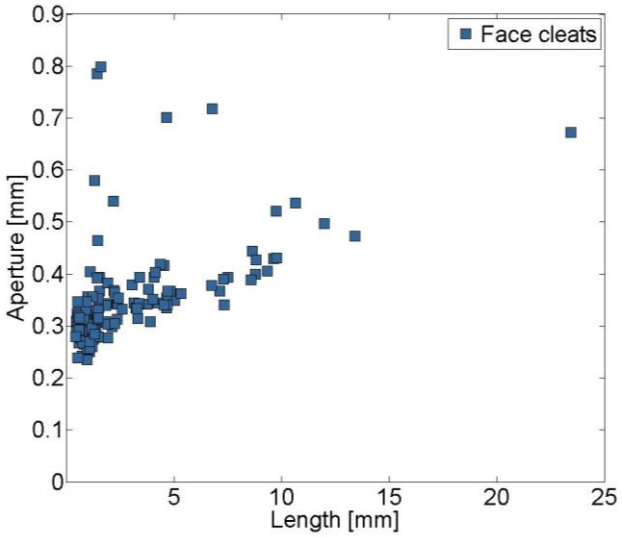

Figure 26 Aperture / length ratio sample H1

4.5. *Cleat spacing*

Sample E1. Based on the gridlines that have been created as explained in 3.2.4, the spacing frequencies are as follows: face cleats I = 0.151 mm^{-1}, face cleats II = 0.126 mm^{-1} and butt cleats = 0.113 mm^{-1}. The cleat spacing distribution is shown in Figure 27. The ratio between the average spacing along the gridlines and the average aperture is plotted in Figure 28a and fitted with a power law in a log log distribution in Figure 28b. For none of the different cleat types, a clear trend between average spacing and aperture can be established.

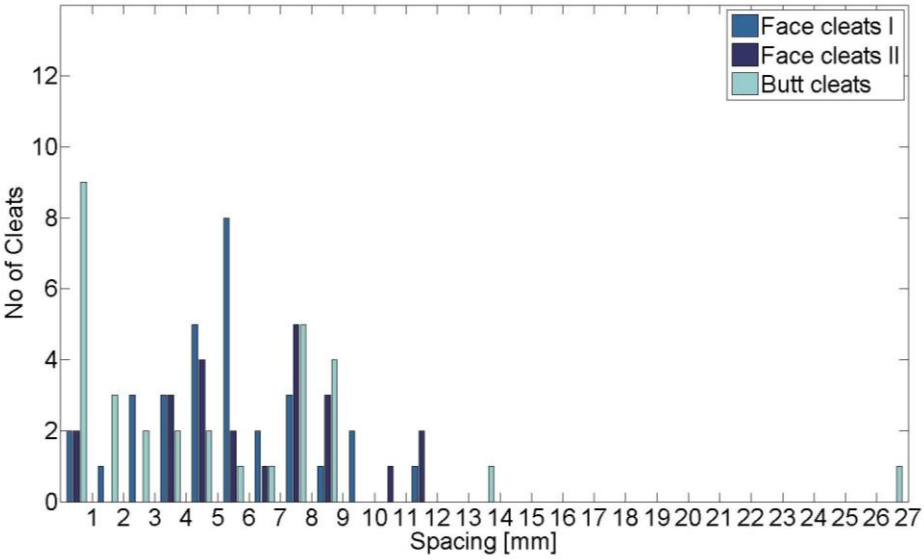

Figure 27 Cleat spacing distribution sample E1

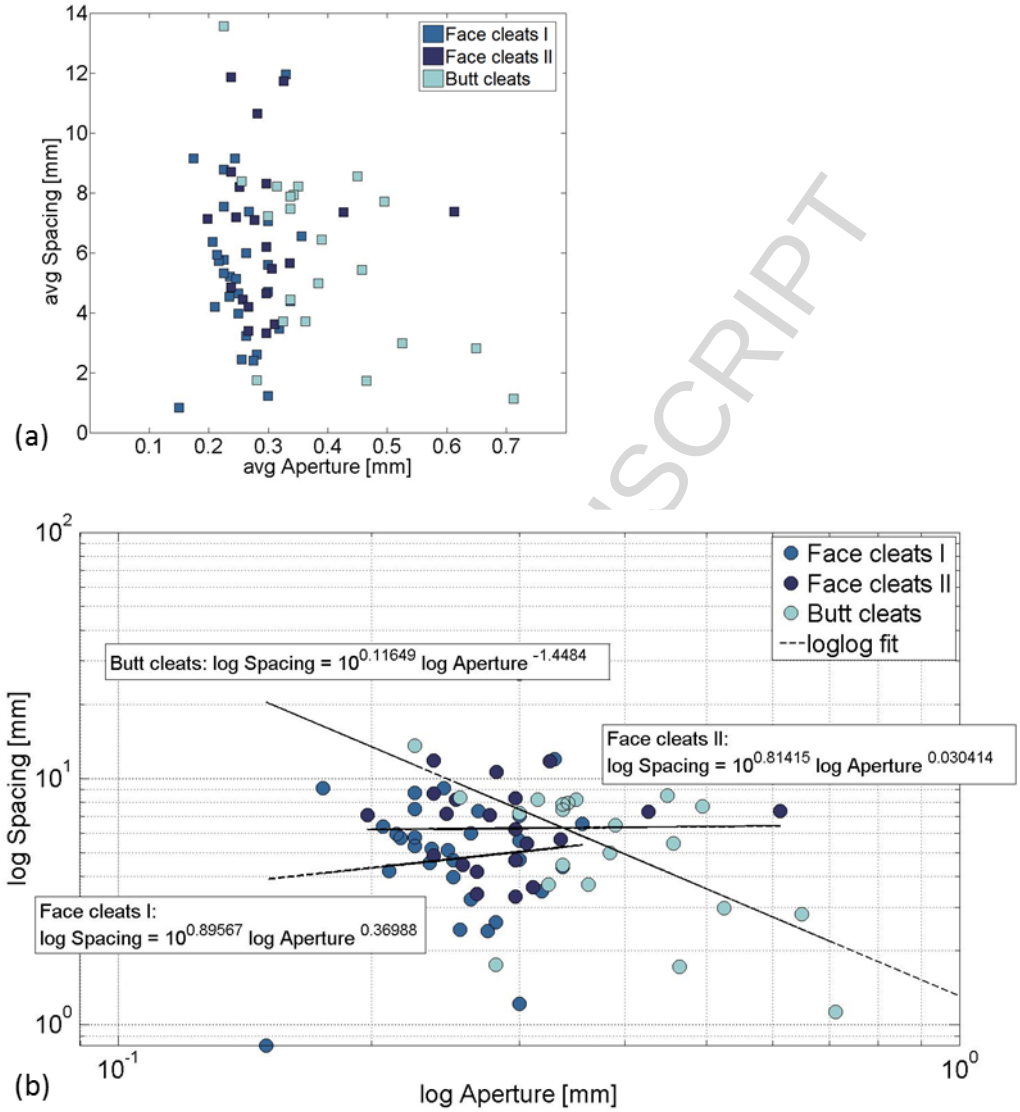

Figure 28 a. Ratio between average spacing and average aperture along gridlines, b. log-log plot of spacing against aperture along gridlines for sample E1

Sample E2. For the face cleats a gridline frequency of 0.1477 mm^{-1} has been found, for the butt cleats the gridline frequency is 0.0998 mm^{-1}. The cleat spacing distribution is shown in Figure 29. No clear relationship between average spacing and average aperture along the gridlines can be established. The plots (Figure 30a and Figure 30b) reveal a random distribution of these two parameters when related to each other.

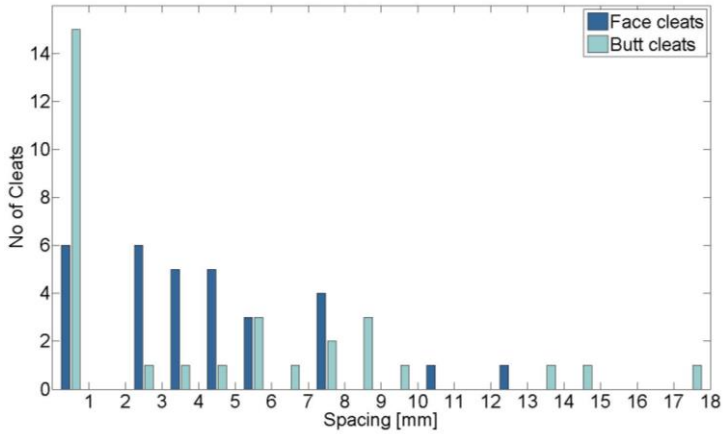

Figure 29 Cleat spacing distribution sample E2

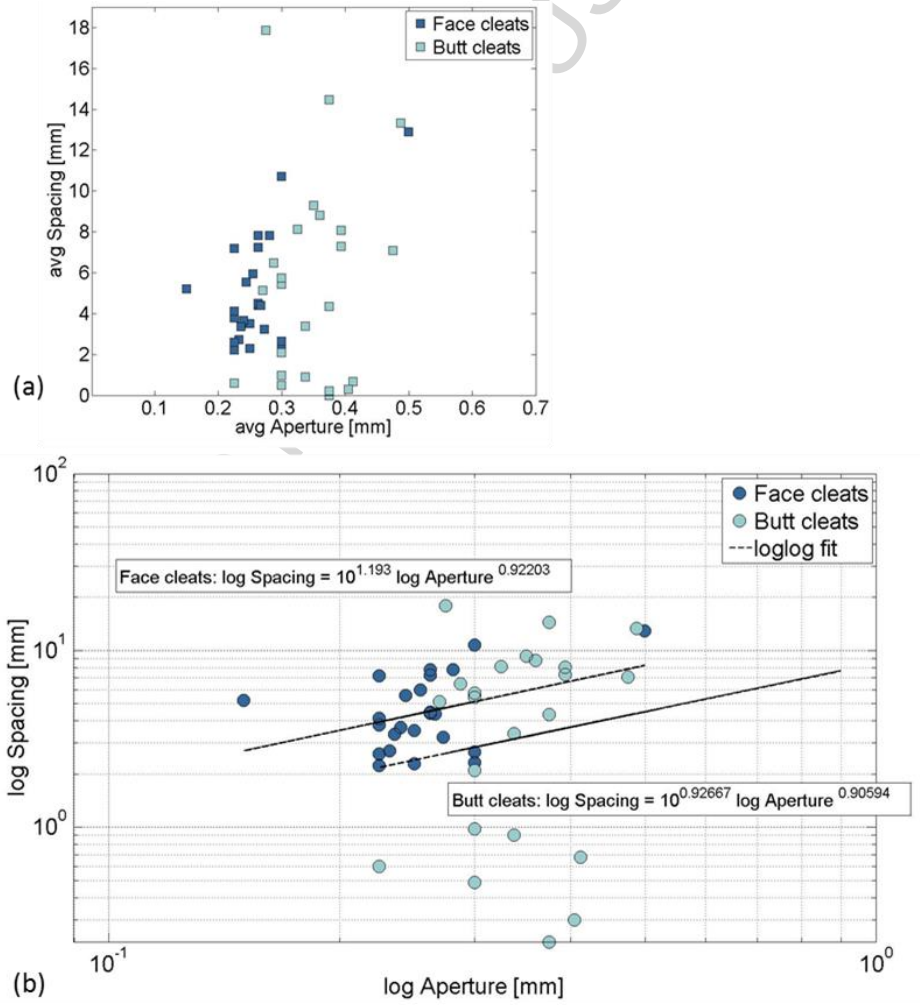

Figure 30 a. Ratio between average spacing and average aperture along gridlines, b. log-log plot of spacing against aperture along gridlinesfor sample E2

Sample H1. The gridline frequency of the face cleats is 0.204 mm^{-1}. The cleat spacing distribution is shown in Figure 31. Ratios between average spacing and average apertures (Figure 32a and Figure 32b) reveal no apparent relationship between these two parameters.

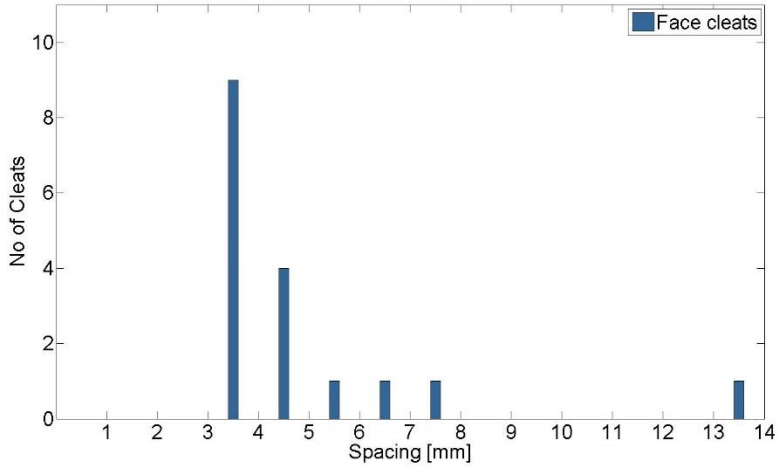

Figure 31 Cleat spacing distribution

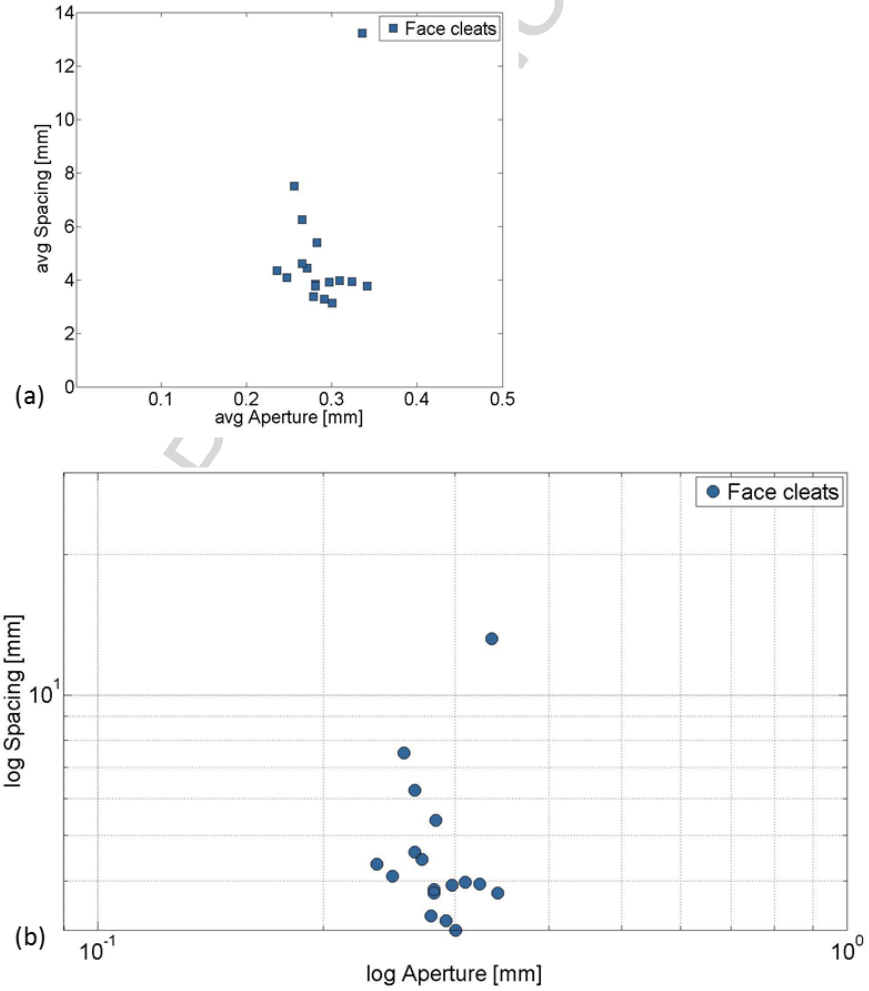

Figure 32 a. Ratio between average spacing and average aperture along gridlines, b. log-log plot of spacing against aperture along gridlines for sample H1

4.6. *Cleat orientation*

Sample E1. The relative orientations for face cleats I and II and butt cleats occurring in the two-dimensional sample are plotted in Figure 33.

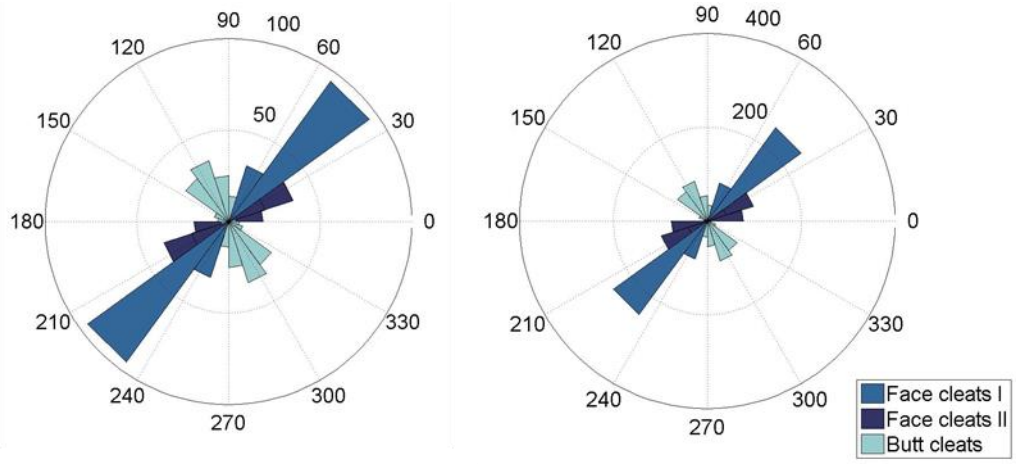

Figure 33 Rose plot of cleat orientations of sample E1: a. total number, b. weighted by their length

Sample E2. Sample E2 is an example of a cleat network with the characteristic perpendicularity between face and butt cleats that has been described by Laubach et al. (1998). The rose plot shows the relative abundance of face cleats compared to the butt cleats (Figure 34).

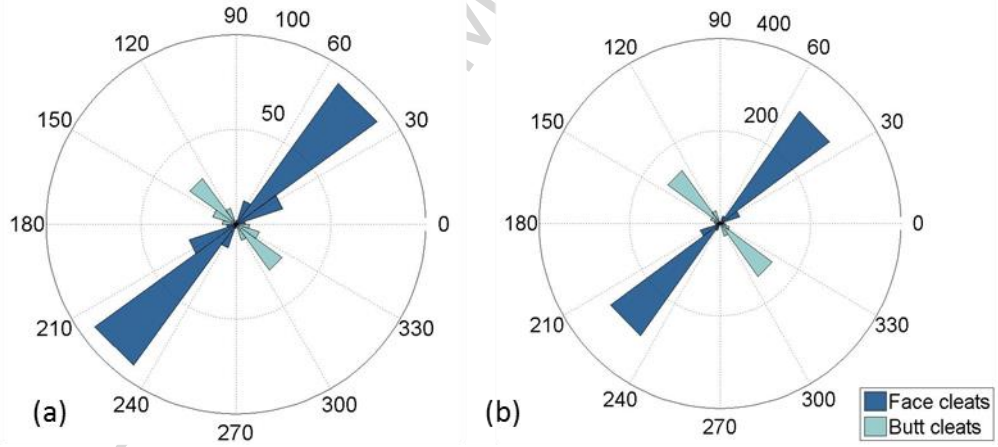

Figure 34 Rose plot of cleat orientations of sample E2: a. total number, b. weighted by their length

4.7. *Cleat connectivity*

Sample E1. As a measure of cleat connectivity, the density of intersections occurring in the image can be used. In total, 197 branch points are observed in the image area. A distinction of all the connected features in the image area is shown in Figure 35, with the Euler characteristic displayed. Negative Euler numbers represent high connectivity sum up to -25.

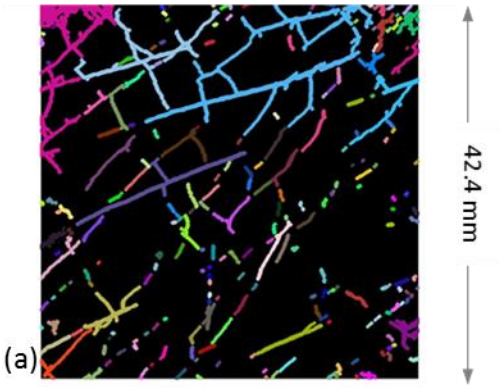

Euler Characteristic	Occurrence
-17	1
-4	1
-3	2
-1	2
0	6
1	207

(b)

Figure 35 a. Connected features of sample E1 distinguished by colours b. occurences of Euler characteristic

Sample E2. The network of face and butt cleats is well connected with a density of intersections given by the number of branch points of 238 in the image area. The connected features are shown in Figure 36, as well as a table of the occurring Euler characteristics. The negative Euler characteristic is summing up to -12.

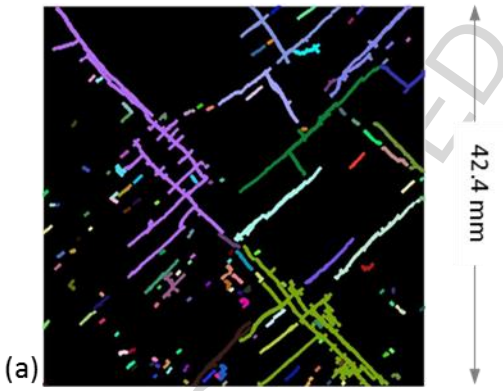

Euler Characteristic	Occurrence
-7	1
-4	2
-1	1
0	2
1	130

(b)

Figure 36 a. Connected features of sample E2 distincted by colours b. occurences of Euler characteristic

5. Discussion

5.1. *Cleat characteristics*

Three different network types of coal cleats have been described based on CT scans taken from coal samples. The classic cleat model with face and butt cleats, therefore, can be extended to a more accurate description as has been proposed by Turner (2015) (Figure 1). Using a MatLab based image processing workflow, we present and characterise three different cleat networks. One sample (E1) shows a geometry with two types of face cleats and one set of butt cleats. Sample E2 reveals a coal network similar to the classic butt/face cleat model. The third sample that is presented (H1) shows parallel face cleats only. The different networks of butt and face cleats found in the examples look similar to those fracture networks in tight gas sandstones explained by Olson et al. (2009) where systematic effects of fracture blockage and length changes are noted and their effects on permeability are investigated.

Cleat aperture has been found to follow a power-law distribution, for butt as well as face cleats. Apertures were found in the range of 0.3 mm to 2.5 mm for butt cleats and 0.25 to 0.75 mm for face cleats. These values are larger than the results presented by Weniger et al. (2016) who measured a maximum aperture of 2.0 mm, and a smallest aperture of 2 µm, with a median of 29 µm. No clear relationship between spacing and aperture could be established. A large range of the cleat spacings that have been measured are smaller than the range of 10-25 mm given as typical numbers in the literature. This might be due to the fact that the cited study (Wang et al., 2009) focused on large-scale major cleats. The image processing based method captured the more common small-scale cleats with spacings of less than a millimetre, as have been described by Dawson and Esterle (2010). This result highlights the usefulness of high-resolution CT-scanning, but also the fact that spacing measurements are limited by the diameter of the core sample. The maximum spacings have been found to be smaller for face cleats (max. 13 mm) than for butt cleats (max. 27 mm).

In all cases, the total number of face cleats outweighed the total number of butt cleats, as did the total length of the face cleats. Gridline frequencies of face cleats are higher than those of the butt cleats. The same holds true for the area sizes, which always follow a power law distribution. While density of face cleats is generally larger than those for butt cleats, intensity values follow no clear pattern when comparing face cleats with butt cleats. As butt cleats are formed to accommodate relaxation of the stress which originally lead to the formation of the face cleat, the lack of a clear pattern regarding cleat intensity could be due to the relaxation of the sample after coring. However, since in this study mineralised cleats are investigated, one can justifiably assume that the influence of relaxation on the presented results is minimal.

Two approaches have been tested to describe the connectivity of the cleat networks: the number of branchpoints, as well as the Euler number. A visual comparison between sample E1 and sample E2 shows a higher connected network in sample 1. However, the number of branchpoints (197) is smaller than the one for sample E2 (238). The Euler characteristics deliver a result matching the visual impression with a higher sum of negative numbers occurring for sample E1.

5.2. *Discussion of the image processing method*

The simplicity of the image processing based approach allows high reproducibility. However, there are some sources of uncertainty that may impact on the resulting cleat network characteristics. As only two dimensions are used the common biases truncation, censoring and trace disconnection are still a concern. The region of interest most likely is smaller than the longest cleat occurring. Therefore, the sampling size is still a serious limitation.

Image processing for geo-materials is an ongoing research topic in different engineering disciplines, with a growing community sharing ideas and the potential to improve measuring techniques constantly. By comparing different current approaches to depict cleat network characteristics, issues related to representativity, reproducibility and resolution can be minimised. For examples, to test the quality of the cleat segmentation and clustering described here, results of other segmentation techniques (e.g., manual, sobel edge detection, watershed segmentation) can be used and compared. As the non-invasive insight into a material is one of the main advantages of CT-scans, the cleat network in a stack of slides can be investigated to characterise cleat connectivity and statistics in 3D. This would allow for the investigation of the relationship of the two-dimensional cleat network statistics with the three-dimensional structure. The derived data can then be used for directional permeability estimations and are therefore useful for the engineering practitioner. The distributions and derived power law exponents can be used as input parameters for geo-mechanical and hydraulical models. The common approach for the modelling of fluid flow in fractures is to randomly generate artificial sets of fractures based on commonly known distributions (De Dreuzy et

al., 2001). However, CT-scans can only give an insight into the cleat pattern of coal after they have been recovered. To date it is still a matter of discussion, if and to what extend the cleats are created during the coring process or if they are already formed in-situ. Generally, straight and systematic cleats are considered to be of natural origin. It is commonly understood that due to relaxation, apertures ex-situ are larger than at depth. The relaxation might also influence the ovality of the core samples and therefore influenced the similarity/difference between face and butt cleat apertures. However, since this study focuses on mineralised cleats, we assume that no drilling-induced fractures were involved. Of importance to the practitioner is the preservation of the core sample orientation during image acquisition and processing. To allow for cleat mapping in the field that could be subject to an up-scaling, the accurate sampling orientation would have to be noted already in the field.

6. Conclusion

We present a solid image processing method to extract main shape features of a cleat network in 2D images of coal samples. A simple criterion for clustering is used: if a gap between two cleats that are aligned along the same axis is smaller than the aperture, they are considered as one cleat and grouped together. With the presented method, the distinction between three different types of cleat geometries is possible that are extending the common definition of face and butt cleats in coal samples. While one sample follows the commonly accepted model of perpendicular face and butt cleats, the second sample shows two sets of face cleats intersected by butt cleats and the third one features parallel face cleats only.

The parameters derived from the scans using the presented method are cleat length, apertures, sizes, intensities, densities, shape parameter, spacing, orientation, and connectivity. The output of the study can serve as an input for the modelling of fluid flow in cleats and geo-mechanical modelling. Usually, artificial sets of cleats are generated based on commonly known distributions of geometrical parameters. Therefore the proposed method is a step towards an accurate description of a real coal cleat network. As the resulting parameters are highly influenced by the quality and resolution of the images used for the analysis, significant improvement can be achieved by using other techniques for capturing the internal structure of samples. One possible method is micro-CT scanning. However, the use of higher resolved measuring techniques comes with the cost of being able to investigate only small sample sizes. One possible solution for this dilemma could be the combination of different methods. Further improvement can be done by using different methods for segmenting the cleat structure. By extending the analysis to several slices along the sample, the database can be extended in order to improve the statistical analysis of the results. The presented paper concentrated on presenting the image processing method with exemplary results of different cleat structures. Future improvement and investigation will concentrate on extending the method to 3D to provide a more detailed and realistic characterisation of the three-dimensional structure of cleats in coal.

7. Acknowledgement

The coal samples used in this analysis were provided by Rio Tinto Coal Australia. The contributions and discussions with Patrick Schmidt of the University of Queensland are gratefully acknowledged. The manuscript has been improved thanks to the valuable input of three anonymous reviewers. This research has been funded by the Australia Coal Association Research Program (ACARP C20022).

8. References

Bonnet, E. et al., 2001. Scaling of fracture systems in geological media. *Reviews of Geophysics*, 39(3), pp.347–383.

Busse, J. et al., 2015. *Detection and description of fracture networks in coal samples for micro-scale flow simulations*, Prague.

Clarke, G., 2007. *Documentation of Significant Geological Features evident within Rio Tinto's Hail Creek Coal Mine*, Queensland.

Clarkson, C.R. & Bustin, R.M., 2011. Coalbed Methane: Current Field-Based Evaluation Methods. *SPE Reservoir Evaluation & Engineering*, 14(1).

Close, J.C., 1993. Natural fractures in coal. In B. E. Law Rice, D.D., ed. *Hydrocarbons from coal*. Tulsa, Oklahoma, U.S.A.: The American Association of Petroleum Geologists, pp. 119–132.

Dawson, G.K.W. & Esterle, J.S., 2010. Controls on coal cleat spacing. *International Journal of Coal Geology*, 82(3–4), pp.213–218.

Dershowitz, W., 1984. *Rock joint systems*. Massachusetts Institute of Technology, Cambridge.

Deza, M.M. & Deza, E., 2009. *Encyclopedia of distances*, Heidelberg: Springer Berlin.

De Dreuzy, J.R., Davy, P. & Bour, O., 2001. Hydraulic properties of two-dimensional random fracture networks following a power law length distribution 1. Effective connectivity. *Water Resources Research*, 37(8), pp.2065–2078.

Dron, R., 1925. Notes on cleat in the Scottish coalfield. *Transactions of the Institution of Minining Engineering*, 70, pp.115–117.

Faiz, M. & Aziz, N., 1992. Porosity and gas sorption capacity of some eastern Australian coals in relation to coal rank and composition. In *Coalbed Methane Symposium, Townsville*.

Galindo-Torres, S.A. et al., 2015. Scaling solutions for connectivity and conductivity of continuous random networks. *Physical Review E.*, 92(4), pp.1–5.

Galindo-Torres, S.A. et al., 2015. Scaling solutions for connectivity and conductivity of continuous random networks. *Physical Review E*, 92, pp.1–5.

Ghaffari, H.O., Nasseri, M.H.B. & Young, R.P., 2011. Fluid Flow Complexity in Fracture Networks: Analysis with Graph Theory and LBM. *arXiv preprint*, arXiv:1107.

Golab, A. et al., 2013. High-resolution three-dimensional imaging of coal using microfocus X-ray computed tomography, with special reference to modes of mineral occurrence. *International Journal of Coal Geology*, 113(0), pp.97–108.

Gonzales, R.C., Woods, R.E. & Eddins, S.L., 2004. Digital image processing using MatLab [Power point slides].

Holwell, M., 2007. Geology at Hail Creek [Power Point slides].

Hooker, J.N., Laubach, S.E. & Marrett, R., 2013. Fracture-aperture sizedfrequency, spatial distribution, and growth processes in strata-bounded and non-strata-bounded fractures, cambrian mesón group, NW argentina. *Journal of Structural Geology*, 54, pp.54–71.

Huy, P.Q. et al., 2010. Carbon dioxide gas permeability of coal core samples and estimation of fracture aperture width. *International Journal of Coal Geology*, 83(1), pp.1–10.

Jing, L. & Stephansson, O., 2007. Fundamentals of Discrete Element Methods for Rock Engineering - Theory and Applications. In *Developments in Geotechnical Engineering*. Developments in Geotechnical Engineering. Elsevier, pp. 365–398.

Karacan, C.Ö. & Okandan, E., 2000. Fracture/cleat analysis of coals from Zonguldak Basin

(northwestern Turkey) relative to the potential of coalbed methane production. *International Journal of Coal Geology*, 44(2), pp.109–125.

Ketcham, R.A. & Iturrino, G.J., 2005. Nondestructive high-resolution visualization and measurement of anisotropic effective porosity in complex lithologies using high-resolution X-ray computed tomography. *Journal of Hydrology*, 302(1–4), pp.92–106.

Khan, F. et al., 2012. 3D simulation of the permeability tensor in a soil aggregate on basis of nanotomographic imaging and LBE solver. *Journal of Soils and Sediments*, 12, pp.86–96.

Klawitter, M., Collins, S. & Esterle, J., 2013. *Coal density and fracture charcterisation by X-ray computerised tomography scanning: a case study of Bowen Basin, Queensland, Australia*, Brisbane: University of Queensland.

Kumar, M. et al., 2010. Visualizing and quantifying the residual phase distribution in core material. *Petrophysics*, 51(5), p.323.

Laubach, S.E. et al., 1998. Characteristics and origins of coal cleat: A review. *International Journal of Coal Geology*, 35(1–4), pp.175–207.

Laubach, S.E., Olson, J.E. & Gale, J.F.W., 2004. Are open fractures necessarily aligned with maximum horizontal stress? *Earth and Planetary Science Letters*, 222(1), pp.191–195.

Long, J.C.S. & Witherspoon, P.A., 1985. The relationship of the degree of interconnection to permeability in fracture networks. *Journal of Geophysical Research: Solid Earth*, 90(B4), pp.3087–3098.

Madadi, M. & Sahimi, M., 2003. Lattice Boltzmann simulation of fluid flow in fracture networks with rough, self-affine surfaces. *Physical Review E*, 67(2), pp.1–12.

Mazumder, S. et al., 2006. Application of X-ray computed tomography for analyzing cleat spacing and cleat aperture in coal samples. *International Journal of Coal Geology*, 68(3–4), pp.205–222.

Nick, K., Conway, M.W. & Fowler, K.S., 1995. The Relation of Diagenetic Clays and Sulfates to the Treatment of Coalbed Methane Reservoirs. In *SPE Annual Technical Conference and Exhibition*. Society of Petroleum Engineers.

Odgaard, A. & Gundersen, H.J., 1993. Quantification of connectivity in cancellous bone, with special emphasis on 3-D reconstructions. *Bone*, 14(2), pp.173–182.

Olson, J.E., Laubach, S.E. & Lander, R.H., 2009. Natural fracture characterization in tight gas sandstones: Integrating mechanics and diagenesis. *AAPG Bulletin*, 93(11), pp.1535–1549.

Ortega, O.J., Marrett, R.A. & Laubach, S.E., 2006. A scale-independent approach to fracture intensity and average spacing measurement. *AAPG Bulletin*, 90(2), pp.193–208.

Pattison, C., Fielding, C. & McWatters, R., 1996. Nature and origin of fractures in Permian coals from the Bowen Basin, Queensland, Australia. *Geological Society,*.

Pratt, W.K., 2001. *Processing Digital Image Processing* Third Edit., Los Altos, California: John Wiley & Sons, Inc.

Priest, S.D. & Hudson, J.A., 1976. Discontinuity spacings in rock. *International Journal of Rock Mechanics and Mining Sciences and*, 13(5), pp.135–148.

Robertson, E. & Christiansen, R., 2006. A Permeability Model for Coal and Other Fractured Sorptive-Elastic Media. In *Society of Petroleum Engineers Eastern Regional Meeting*. pp. 11–13.

Rosin, P.L., 2001. Unimodal thresholding. *Pattern Recognition*, 34(11), pp.2083–2096.

Rouleau, A. & Gale, J., 1985. Statistical characterization of the fracture system in the Stripa granite, Sweden. *International Journal of Rock Mechanics and Mining*.

Scott, A.R., 2002. Hydrogeologic factors affecting gas content distribution in coal beds. *International*

Journal of Coal Geology, 50(1–4), pp.363–387.

Turner, L.G., 2015. *Chemical Stimulation Techniques for Increasing the Permeability of Coal Seams*. The University of Queensland.

Vogel, H.J. & Roth, K., 2001. Quantitative morphology and network representation of soil pore structure. *Advances in Water Resources*, 24, pp.233–242.

Walsh, J.J. & Watterson, J., 1993. Fractal analysis of fracture patterns using the standard box-counting technique : valid and invalid methodologies. , 15(12), pp.1509–1512.

Wang, G.X., Massarotto, P. & Rudolph, V., 2009. An improved permeability model of coal for coalbed methane recovery and CO2 geosequestration. *International Journal of Coal Geology*, 77(1–2), pp.127–136.

Weniger, S., Weniger, P. & Littke, R., 2016. Characterizing coal cleats from optical measurements for CBM evaluation. *International Journal of Coal Geology*, 154–155, pp.176–192.

Witherspoon, P.A. et al., 1979. Validity of cubic law for fluid flow in a deformable rock fracture. *Water Resources Research*.

Wolf, K.H.A.A. et al., 2008. Determination of the cleat angle distribution of the RECOPOL coal seams, using CT-scans and image analysis on drilling cuttings and coal blocks. *International Journal of Coal Geology*, 73(3–4), pp.259–272.

Highlights

- An Image processing workflow to characterise coal cleat networks is introduced
- Workflow is based on the distinction of perpendicular face and butt cleats
- Geometric parameters for three different cleat networks are deduced